AD-A115 885 CAMBRIDGE UNIV (ENGLAND) DEPT OF ENGINEERING F/G 13/13
VERIFICATION OF THE NEWARK ANALYSIS OF PERMANENT DISPLACEMENTS --ETC(U)
NOV 81 B L KUTTER DAJA37-79-C-0387

UNCLASSIFIED NL

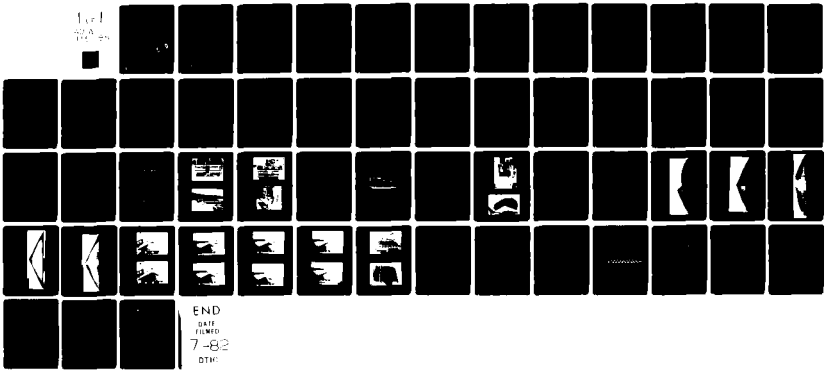

END
DATE FILMED
7-82
DTIC

UNCLASSIFIED

R&D 2755-EN

SECURITY CLASSIFICATION OF THIS PAGE (When Data Entered)

AD A115885

REPORT DOCUMENTATION PAGE		READ INSTRUCTIONS BEFORE COMPLETING FORM
1. REPORT NUMBER	2. GOVT ACCESSION NO. AD-A115 885	3. RECIPIENT'S CATALOG NUMBER
4. TITLE (and Subtitle) Verification of the Newmark Analysis of Permanent Displacements of Earth Embankments subject to Earthquake Loads on a Geotechnical Centrifuge		5. TYPE OF REPORT & PERIOD COVERED Final Technical Report July 1979 - October 1981
		6. PERFORMING ORG. REPORT NUMBER
7. AUTHOR(s) Bruce L. Kutter		8. CONTRACT OR GRANT NUMBER(s) DAJA37-79-C-0387
9. PERFORMING ORGANIZATION NAME AND ADDRESS Engineering Department Cambridge University Cambridge CB2 1PZ		10. PROGRAM ELEMENT, PROJECT, TASK AREA & WORK UNIT NUMBERS 6.11.02A-1T161102BH57-01
11. CONTROLLING OFFICE NAME AND ADDRESS USARDSG-UK Box 65 FPO NY, NY 09510		12. REPORT DATE November 1981
		13. NUMBER OF PAGES 54
14. MONITORING AGENCY NAME & ADDRESS (if different from Controlling Office)		15. SECURITY CLASS. (of this report) Unclassified
		15a. DECLASSIFICATION/DOWNGRADING SCHEDULE

16. DISTRIBUTION STATEMENT (of this Report)

Approved for Public Release - Distribution unlimited

17. DISTRIBUTION STATEMENT (of the abstract entered in Block 20, if different from Report)

DTIC ELECTE JUN 22 1982 S D H

18. SUPPLEMENTARY NOTES

19. KEY WORDS (Continue on reverse side if necessary and identify by block number)

Soil mechanics, Newmark Analysis, embankment failure, earthquakes, Geotechnica centrifuge, strain softening, embankment base acceleration, sliding block analysis

20. ABSTRACT (Continue on reverse side if necessary and identify by block number)

The objective was verification of the Newmark (1965) sliding block analysis to predict permanent displacements of earth dams subjected to earthquake loading. The tests were conducted on a new "Bumpy Road" shaking table aboard the Cambridge University Geotechnical Centrifuge. Clay embankment models of triangular cross section with 1:2 slopes that represent prototypes of 6.9 m height were each submitted to between three and six earthquakes. →

DTIC FILE COPY

DD FORM 1 JAN 73 1473 EDITION OF 1 NOV 65 IS OBSOLETE S/N 0102-LF-014-6601

UNCLASSIFIED

SECURITY CLASSIFICATION OF THIS PAGE (When Data Entered)

20/...

The sliding block calculations consistently under estimated displacements; however, relative errors in displacements were smaller for large than small earthquakes. The yield of clay at stresses below the shear strength, dynamic magnification of base acceleration and strain softening during shaking are cited as factors contributing to unconservative predictions of displacement.

Another, unexpected mode of embankment failure was observed: strain softening and pore pressure generation during one test caused a slope failure 3.5 s (two hours in prototype terms) after the model earthquake. The displacement during this slump was about 2.8 m in prototype terms - on the order of ten times the displacements which occurred during any actual earthquake.

Final Report on the Verification of the Newmark Analysis of Permanent Displacements of Earth Embankments subject to Earthquake Loads on a Geotechnical Centrifuge

B L Kutter
Cambridge University Engineering Dept.
November 1981

1. SYNOPSIS

Five additional embankment models have been tested to complete a research project on the verification of the Newmark (1965) sliding block analysis to predict permanent displacements of earth dams subjected to earthquake loading. The tests were conducted on a new "Bumpy Road" shaking table aboard the Cambridge University Geotechnical Centrifuge. Clay embankment models of triangular cross section with 1:2 slopes that represent prototypes of 6.9 m height were each submitted to between three and six earthquakes. The sliding block calculations consistently underestimated displacements; however, relative errors in displacements were smaller for large than small earthquakes. The yield of clay at stresses below the shear strength, dynamic magnification of base acceleration and strain softening during shaking are cited as factors contributing to unconservative predictions of displacement.

Another, unexpected mode of embankment failure was observed: strain softening and pore pressure generation during one test caused a slope failure 3.5 s (two hours in prototype terms) after the model earthquake. The displacement during this slump was about 2.8 m in prototype terms - on the order of ten times the displacements which occurred during any actual earthquake.

2. INTRODUCTION

The purpose of this research was to test the validity of using Newmark sliding block calculations to predict permanent deformations of clay embankments during earthquakes. In view of the unpredictability, unrepeatability and infrequency of real, large earthquakes, it is valuable to conduct model tests to improve our understanding of the behaviour of earth structures during base shaking.

Soil models at one gravity can help to supplement field data but suffer from the drawbacks of using either very large (difficult to prepare) models or small models at very low stress levels. Centrifuge modelling allows the researcher to produce small (easy to prepare) models at the correct stress levels. Hence, it is a useful tool for producing experimental data to test, verify and develop our understanding of the dynamic behaviour of soil.

It was proposed to conduct a series of model tests utilizing an existing shaking table aboard the Cambridge Centrifuge. It was proposed that by varying the clay shear strength, the centrifuge speed, and the earthquake magnitude, the deformation during a range of combinations of yield acceleration and base acceleration could be measured for comparison with sliding block theory.

For the five initial tests reported in the first progress report (M. Phil. thesis, B.L. Kutter) it was attempted to keep approximately the same shear strength in all models and only to vary the centrifuge acceleration and the earthquake acceleration. These tests gave some good results but also revealed problems and suggested possible improvements in the test procedure as well as making clear the difficulty of carrying out some tests suggested in the proposal:

(1) It is impractical to test models with yield accelerations of 5% of the centrifuge accelerations or less. This would imply static factors of

safety on the order of 1.1 which besides being atypical of real dams, could result in ruining a model due to creep, small errors in centrifuge speed or clay shear strength.

(2) The geometry of models used for the initial tests was undesirable in two respects. Firstly, the embankment slopes were steeper than those typical of earth dams. Secondly, there was only one sloping face, and the clay was confined on the other side by the wall of the shaking table. Although this wall was well clear of "static" (non-earthquake) failures, earthquake shear zones were found to be more reclined and did actually intersect this clay wall boundary.

(3) Using the spring mass resonant shaking table on clay specimens was difficult since only one earthquake could be released per centrifuge flight. In addition, the catch mechanism could not be cocked until just before a model earthquake since premature firing of the earthquake would occur in a matter of tens of minutes after cocking. These conditions made it impossible to achieve complete pore pressure equilibrium before the earthquakes and also necessitated numerous stop-start centrifuge cycles in the course of model testing.

For these and other reasons, a new actuating system was developed for additional tests. The new apparatus afforded much more versatility but also introduced one different test restriction. It was not capable of imposing earthquakes greater than 40% of the centrifuge acceleration. This precluded the possibility of performing the large earthquakes originally proposed at the low centrifuge accelerations.

The new apparatus allowed construction of larger embankment models with two sloping faces, each with 1:2 slopes. In order to limit the number of new variables it was considered desirable in the additional tests to again hold the clay shear strength constant. Since the magnitude of the earthquakes, the centrifuge acceleration, and the frequency of vibration

were the easiest and most accurately adjustable variables, these were the only parameters that were varied in the additional tests.

3. THE BUMPY ROAD APPARATUS

The apparatus was conceived by P.W. Turner and the design was carried out jointly by P.W. Turner and B.L. Kutter. It operates by forcing a wheel on the centrifuge arm to follow a curved steel track that is attached to the wall of the centrifuge pit. The wheel vibrations are then transmitted through a crankshaft and slider mechanism to vibrate the soil model tangentially relative to the centrifuge. Several earthquake tests on board the Cambridge centrifuge have been conducted using a spring mass resonant actuator designed by Morris (1979), however this apparatus was limited in sample dimension, and only a single earthquake could be released during a centrifuge flight.

The Bumpy Road actuator provides improved dynamic motions to centrifuge samples with the following features:

* 20 g "earthquake" accelerations.
* Vibration frequencies up to about 150 Hz.
* Capacity for 135 kg models.
* Centrifuge accelerations up to 100 g.
* A soil container with approximate dimensions of 0.9 × 0.48 × 0.22 m (length:width:height) to accommodate embankment dam models.
* Provision for viewing a cross section of the models during flight by using flash photography.
* Ability to release several earthquakes during flight without stopping the centrifuge.
* Capability of in-flight variability of earthquake magnitude.
* Provision for changing earthquake waveform by changing the track on the centrifuge wall.

Two schematic views of the system are shown in Figure 3.1. The track (1) extends over about 1/3 of the circumference of the centrifuge pit and is machined to a prescribed waveform by a numerically controlled milling

machine. As the wheel (2) follows the track the crank (3) and shaft (4) are rotated dynamically. The wheel is held against the track by the double acting pneumatic jack (5). The vibration take off slider (6) can be moved to an eccentric position relative to the shaft by an electric motor and screw jack (7) to provide any desired ratio of package displacement to wheel displacement between 0.0 and 0.2. The slider itself imparts the tangential dynamic loads to an actuating beam (8) which rests on linear roller bearings (9). The beam is bolted to a rack (10) which engages with a matching rack on the swinging platform (11). In plan view looking vertically into the centrifuge pit, the model dam (12) is enclosed on the ends by aluminium alloy walls (13). Slumping soil from a model can be allowed to fall into the overflow chambers (14) to prevent the build up of soil against the end walls. The model is viewed in cross section through polycarbonate windows.

The platform itself is suspended by tangentially flexible straps (16) from torsion bars (17). As the centrifuge acceleration is increased from zero the package swings up until the matching racks become aligned. The torsion bars allow the package to move radially outward relative to the centrifuge arm (18) until the matching racks engage causing the additional centrifugal load to be transferred to the end of the arm through the linear roller bearings.

The tracks are fixed to the wall by fifteen brackets (19) which are in turn fixed to the wall (20) by Rawl Bolts. The bracket spacing is ten degrees of arc of the centrifuge.

The pneumatic system, extremely simplified in figure 3.1 is represented by two reservoirs (21) and two solenoid valves (22) and (23). Part of the pneumatic system is actually mounted at the centrifuge axis. There is an electronic triggering system which synchronises the opening and closing of the solenoid valves with the position of the arm of the

centrifuge relative to the track. So, at the push of a button in the console room, valve (23) is closed and (22) is opened, pulling the wheel out to follow the track for a single revolution. Then (23) is opened and (22) is closed so that the wheel is pushed in to miss the track on subsequent passes. Photographs of the assembled apparatus from various points are shown in Figures 3.2a to 3.2d.

4. INITIAL TESTS: SUMMARY OF RESULTS

A relationship between normalised displacement and the ratio of yield accelerations k_y to base accelerations k_m was developed for sinusoidal base acceleration and is shown in figure 4.1. The predictions of displacements using this relationship for the initial tests on the spring mass actuator consistently underestimated measured displacements. However, at the conclusion of the initial tests it was unclear whether the errors in prediction were a result of deficiencies in the sliding block calculations or deficiencies in the soil models. Evidence from radiographs indicated that the assumption that a distinct rupture plane forms during sliding was not accurate. But the importance of this inaccuracy could not be evaluated.

The radiograph for model BK-5 shown in figure 4.2 illustrates the difference between dynamic deformations (which occur in a wide band) and static failure (which occurs on a rupture surface).

Sample BK-5 was first subjected to earthquake deformation which occurred on the wide band that intersects the left side of the photograph. After the earthquake the centrifuge acceleration was increased until a "static" slip occurred on the very distinct circular arc that intersected the top surface of the specimen.

There are many soil properties which influence the tendency to form rupture surfaces. But, in this case the reason for the differences between dynamic and static mechanisms is: for static (constant) loading, failure occurs when the factor of safety is one, so that soil only on the most critical slip surface is subjected to failure stresses and deformation is confined to this surface; in contrast, dynamic loading can produce factors of safety much less than one for a short time. During this time, deformation occurs on a band of slip surfaces which all have factors of safety less than one.

In spite of the discrepancy between assumed and observed mechanisms, sliding block displacement predictions seemed reasonable. However, the fact that predictions are highly sensitive to the assumed value of soil strength had to be taken into account. To demonstrate this point, consider an example. A sliding block with a yield acceleration of k_y g of 0.1 g rests on an inclined 1:2 cohesive slope (see figure 4.3). A single horizontal sinusoidal acceleration pulse of amplitude k_m g at a frequency of 1 Hz is applied to the base of the model. Now consider the error in displacement predictions during the single acceleration pulse if the predictions are based on a 5% overestimate of shear strength (errors of 5% in the determination of shear strength would not be unusual). For a large sine pulse with $k_y/k_m = 0.2$ one would predict a displacement of 400 mm and would observe 460 mm, a 15% unconservative error. For one small sine pulse with $k_y/k_m = 0.9$ a displacement of 1.0 mm would be predicted and 17 mm would be observed, a 1600% unconservative error. Relative error tends to be larger for small pulses that barely exceed the yield acceleration. This fact makes it difficult to test and compare analytical techniques based on existing field evidence of measured displacements during relatively small earthquakes. The sensitivity of dynamic displacements to strength is the nature of the problem, not of the analytical technique and therefore should not necessarily be considered a drawback of sliding block type calculations.

In conclusion, the relative importance of all assumptions of an analytical technique should be kept in mind. The assumption that a distinct failure plane forms, albeit inaccurate, may be less significant than inaccurate characterisation of soil strength. Centrifuge modelling allows one to conduct a repeatable series of tests helping us to keep these considerations in the proper perspective.

5. BUMPY ROAD TESTS: PREPARATION AND PROCEDURE

All of the model earthquake tests reported here were conducted on embankments of triangular cross section, with 1:2 slopes. The models were trimmed from blocks of kaolin clay consolidated in a rectangular tub to a vertical stress of 124 kPa. The blocks of clay were extruded (see figure 5.1) and then trimmed to the desired profile (see figure 5.2). Sample dimensions and typical transducer locations are shown in figure 5.3 and 5.4. Some pore water pressure transducers were suspended in the clay at the time of pouring the slurry into the consolidometer. Other pore water pressure transducers were inserted along with accelerometers and LVDT resting pads after trimming the sample.

Lead powder threads were inserted into the specimens before testing to allow post test x-radiography to reveal the internal deformation mechanisms caused by earthquakes. Post test radiographs are shown in figures 5.5a to 5.5e. Silver coated nylon markers were placed in grids at 10 mm spacing to enable in flight photographs to reveal the deformation patterns at the specimen boundary. Figures 5.6a to 5.8b are examples of photographs which were taken at various stages during the centrifuge tests. For more information about specimen preparation techniques refer to the first progress report (M. Phil. thesis, B.L. Kutter) written for this proposal or B.L. Kutter's forthcoming Ph.D. thesis.

Post test photographs of model C are shown in figures 5.9a to 5.9b, not only because of the dramatic failure, but to give the reader a feel for the appearance of an instrumented model.

The basic test procedure was to bring the centrifuge up to the test speed then fill the reservoirs to the desired height and allow the pore water pressures to come into equilibrium. After each earthquake was released the sample was allowed to consolidate before the next earthquake. The magnitude of successive earthquakes was adjusted if desired. It is

important to allow the water pressure in a model to come into equilibrium if accurate estimates of shear strength are to be deduced.

Table I summarises the characteristics of the 5 models tested on the Bumpy Road. Most of the model tests simulated a 6.9 m high embankment shaken at a prototype frequency of 1.52 Hz (tests A, B, C, D). Models A and B were tested at 80 g and were therefore 2.25 times smaller than Models C and D which were tested at 35.6 g. Because of the scaling relationship for dynamic centrifuge modelling (see first progress report) models A and B had to be shaken at a higher frequency than C and D, and were therefore conducted with a bumpy road track that had a smaller wavelength. Model E was a slightly larger model than C and D and was tested at 35.6 g on the same wavelength track to test the effect of varying the prototype frequency from 1.52 to 2.28 Hz.

Another variation from the standard frequency and model scale were tests AIV, the fourth earthquake on Model A and test CV, the fifth earthquake on Model C. These tests were conducted after rapidly increasing the centrifuge to 1.25 times the consolidation acceleration and releasing an earthquake before the sample had a chance to consolidate.

6. BUMPY ROAD TESTS: SOME RESULTS AND ANALYSIS

6.1 INTRODUCTION

This section begins with a description of data collected during two model earthquakes. The first one to be discussed is test BI, the first earthquake on one of the small models at 80 g. The second to be discussed is from test DI, the first earthquake on one of the large models tested at 35.6 g.

The section continues with a discussion of the determination of the soil shear strength and the yield acceleration. Using these parameters, sliding block displacements were calculated and compared with measured displacements. Reasons for the underprediction of displacements by the theory are discussed.

The last part of this section discusses the delayed failure of model C, approximately 3.5 seconds after earthquake CV.

Data picked off magnetic tape records or digital data logger records is summarised in Table II. Base and crest peak filtered acceleration, net crest settlement and lateral displacement of the slope faces at mid-height are listed for every earthquake.

Before beginning this analysis it is useful to discuss the repeatability of the model tests, and to demonstrate the agreement between model tests at different scales. Models A and B were small models and were shaken at 80 g centrifuge acceleration. Models C and D were 2.25 times larger and were tested at 35.6 g. The bumpy road track was changed after model tests A and B so that the frequency of vibrations on all four models was scaled according to the dynamic centrifuge modelling laws. All four models represented 6.9 m high embankments that were shaken at 1.52 Hz. The response of all four models should then be similar - since they represent the same prototype, all aspects of the dynamic behaviour should be related by the scaling laws. Testing the scaling laws by constructing models of different scales that represent the same prototype is called "modelling of models".

One aspect of the agreement between the models of different scale has been investigated and is illustrated in figure 6.1. The prototype crest settlement is plotted as a function of peak base acceleration. It is seen that all four models that were shaken at a prototype frequency of 1.52 Hz and had the same prototype height fall on the same curve. Despite the fact that the earthquake amplitudes were not uniform, and were noticeably different for the tests at 35.6 g and 80 g, the agreement is very encouraging.

6.2 DESCRIPTION OF TYPICAL TEST DATA

Examples of the data collected during the model earthquakes are shown in figures 6.2 and 6.3.

Figure 6.2 is the result of the first earthquake on model B (see figure 5.3 for transducer locations). The three base accelerations recorded in figure 6.2a all show very similar wave forms and amplitudes. The acceleration at mid-height in the clay shows some evidence of high frequency vibration during the initial smaller amplitude pulses and shows an attenuation of the sharp peaks of acceleration during the larger amplitude pulses. The horizontal crest acceleration is of a greater amplitude than that for the acceleration at mid-height, it also exhibits a more pronounced high frequency component during the initial earthquake pulses. This high frequency component is due to resonance of the embankment. During the large pulses, the crest acceleration is rounded or chopped off at the peaks due to yielding of the embankment. This yielding causes a reduction of the effective soil modulus and an increase of damping, consequently, the high frequency ringing of the embankment disappears. The vertical acceleration at the crest of the embankment also exhibits a high frequency response during the initial pulses of the earthquake, but again this high frequency response is lost during the large acceleration pulses while the embankment

yields and acceleration pulses of a frequency similar to the basic driving frequency appear.

Figure 6.2b shows the crest settlement and the horizontal displacement of the two slope faces measured half way up the slope. The pore pressure transducers at (11) and (12) H are not responding to the dynamic pressures, probably due to air coming out of solution from the water while the specimen sat under 40 kPa pore water suctions during preparation. However, the transducer at (13) ~~height~~ is responding to the dynamic loading and displays a generation of positive pore pressure.

Figure 6.3 shows the acceleration and displacement response of the first earthquake on model D at 35.6 g (see figure 5.4 for transducer locations). The amplitude of the base acceleration is more uniform than that for the tests at higher frequency (tests A and B). As for the earthquakes on the small models, we see some higher frequency response of the accelerometers in the embankment during the first pulse. The crest accelerations have flattened peaks due to yielding of the clay.

All of the displacement transducers reveal an acceleration in the rate of deformation at about the middle of the earthquake despite the fact that the base accelerations are actually reducing in amplitude throughout the earthquake. This is perhaps caused by softening of the clay during the quake due to pore water pressure generation and/or remoulding. Figure 6.3 shows the pore pressure response at three locations in the embankment. The transducer (10) (on figure 5.4) near the bottom of the embankment shows a positive pore pressure generation of about 25 kPa compared to a total overburden of about 84 kPa. The transducer at (10) also exhibits a frequency response of twice the base shaking frequency - possibly due to the soil going through a contraction/dilation cycle every time the shear stress is reversed. The transducer (11) responds cyclically with gradually increasing amplitude but does not seem to have a permanent offset. The transducer at

(12) shows a small cyclic response and a gradual build up of pore pressure to about 16 kPa and a slow decay.

6.3 DETERMINATION OF THE YIELD ACCELERATION

The yield accelerations of the models were determined from results of a slope stability analysis program. The program was based on the method of slices outlined by Morgenstern and Price (1965) and has been modified to accommodate constant inclined body forces due to lateral acceleration during an earthquake. First, the shear strength was back-calculated by comparing the results of a computer run without earthquake loading with the results of the static failure of model A. This model was consolidated at 80 g after a series of four earthquakes and the speed of the centrifuge was gradually increased (over about four minutes) until it failed at 122 g due to the increased centrifuge acceleration body forces. Hence it was known that the factor of safety was 1.0 at 122 g. The factor of safety of the embankment at 80 g was then 122/80 = 1.53. From this known factor of safety and the results of the computer analysis, the undrained shear strength could be calculated to be 19 kPa. Results of repeated computer runs with horizontal acceleration coefficients of 0.1, 0.15, 0.2, and 0.25 and the known shear strength are plotted in figure 6.4 as factor of safety versus earthquake acceleration coefficient. From this figure it was possible to determine that the yield acceleration coefficient (corresponding to a factor of safety of 1.0) was $k_y = 0.2$.

The height of a prototype slope is proportional to the centrifuge acceleration. The factor of safety against failure of an undrained cohesive slope on board the centrifuge is therefore inversely proportional to the centrifuge acceleration since F.S. $Cu/\gamma h$. So, for the centrifuge tests at 25% greater centrifuge acceleration (tests AIV and CV) the factor of safety against "static" slip is 1.53/1.25 = 1.22. The factor of safety corresponding to any lateral earthquake acceleration coefficient is also

reduced by 25%. Therefore, the lateral acceleration coefficient that produced a factor of safety of 1.25 for the 6.9 m slopes will produce a factor of safety of 1.0 for the 8.6 m high slopes. Using the above reasoning, a relationship between factor of safety and lateral acceleration coefficient for the 8.6 m high embankments was determined by scaling down the relation for 6.9 m high slopes. The extrapolated relationship is dotted on figure 6.4, the yield acceleration can be picked off at about 9% of the centrifuge acceleration.

6.4 PREDICTIONS OF DISPLACEMENTS USING THE SLIDING BLOCK MODEL

The base acceleration data from FM magnetic tape for four earthquakes was digitized and stored on floppy disc. A Fortran program was written to calculate sliding block displacements for the digitized earthquakes. The output of the program gives relative velocities and relative displacements of the sliding block. The results of these calculations are summarized in Table III. Plots of predicted relative velocity and displacement with time are shown in figures 6.5 and 6.6. These plots were obtained using a reduced shear strength, reasons for reducing the shear strength for these calculations will be explained later. These plots are included to demonstrate the kind of output that can be obtained from the program.

The results of the calculations are compared with measured relative displacements of the models in figures 6.5, 6.6. and 6.7 and in Table III. In each of the model tests there was either one or two displacement transducers measuring the horizontal displacement of the slope faces at mid height. The measured displacements that are compared with predictions in Table III are not corrected to account for the fact that horizontal, near surface displacements are not identical to the displacements of the centre of gravity of the sliding soil mass. Because the transducers were not aligned exactly in the direction of relative motion, and were not anchored at the centre of gravity of the sliding soil, they may have recorded displacements of

only 80% to 90% of the relevant displacement. Because this correction is indefinite, in addition to being small compared with the errors in predictions, it was preferable to present the unmodified data in the tables and figures of this report. Figure 6.7 is a graphic presentation of the data in table III. The model displacements have been converted to prototype displacements and plotted against the error ratio: predicted displacement/measured displacement.

For tests BI, CIII and DI, the predicted displacements were all less than 10% of the measured displacements. Only for test CV, which involved much larger displacements, were the predictions within a factor of two of the measured displacements. There are several possible causes for this large discrepancy:

(1) Plastic deformation occurs at stresses below the shear strength.

(2) Dynamic magnification of accelerations in the embankment produces larger accelerations and inertia forces.

(3) The soil strain softens during the earthquake.

(4) The sliding block model restricts shear to a single slip surface whilst in the centrifuge models, the deformation has a greater degree of freedom.

The fourth of the listed causes requires more study to evaluate its importance. There is evidence to suggest that the first three causes did contribute to the discrepancy between predictions and measurements. These causes will be discussed below.

(1) Soil is an elasto-plastic work hardening/softening material. It does exhibit plastic strains at stresses below the shear strength. Undrained shear of Kaolin requires 2% to 15% shear strain to mobilise the undrained shear strength in monotonic loading. A 1% shear strain might mobilise only about 50% of the shear strength of lightly over-consolidated Kaolin (Sketchley, 1973). A 1% shear strain distributed over a 20 mm thick shear band could produce 0.2 mm of displacement per pulse of acceleration, or 2.0 mm

over the 10 pulse earthquake. This is of the same order as the displacements recorded in Tables II and III. An important improvement of the sliding block model would be to account for the non-linear nature of the soil instead of assuming rigid plastic behaviour.

One method of accounting for yield at stresses below the shear strength would be to use a non-linear force displacement relation in the sliding block analysis. A simpler method would be to use a reduced but constant strength in the analysis. This involves the selection of an arbitrary reduced strength. Some calculations were conducted using a reduced strength of 90% of the actual strength. The results of these calculations are also listed in Table III, and are used for the plots of figure 6.5 and 6.6. Using the reduced strength improves displacement predictions considerably, especially for the earthquakes that produced small deformations. However, for test CV, the reduced strength results in an overestimation of displacements. These results suggest that the effective reduced strength depends on the magnitude of the mobilised stresses and displacements.

(2) Dynamic magnification of accelerations by factors between 1.25 and 2.0 was measured in every earthquake test. Because the base and crest motions often had different frequency content, it was difficult to compare their amplitudes by simply picking values off plots such as figures 6.2 and 6.3. The values of base and crest acceleration recorded in Table II were taken from filtered acceleration records (filtered by eye only) - the high frequency spikes like those in the base acceleration traces of figure 6.2 were disregarded.

Further, more objective analysis will be made using Fourier Spectra and comparisons of base and crest velocities rather than accelerations in order to evaluate the importance of magnification.

(3) During the earthquakes, pore pressures are generated and the soil may be partially remoulded. This may cause a reduction in the yield acceleration and an increased rate of deformation as the earthquake progresses. The

comparison between predicted and measured displacements during earthquake DI in figure 6.6 (using a reduced strength) demonstrates a phenomenon that could be explained by strain softening. As the earthquake progressed, the amplitude of the base acceleration actually decreased. In the displacement prediction, this was manifested as a reduction in the rate of displacement during the latter half of the earthquake. But, the rate of measured displacements actually increased as the earthquake progressed.

6.5 DELAYED FAILURE AFTER EARTHQUAKE CV

The most catastrophic of the observed failures caused by base shaking was that after test CV. This model sustained large deformations (about 8 mm) during the earthquake. Then, about 3.5 seconds after the earthquake a collapse occurred during which about 70 mm of displacement occurred. The results of the delayed failure are shown in the radiograph of figure 5.5c and the photographs of figures 5.7d and 5.9. Figure 6.8 shows some transducer readings between the time of the earthquake and the "static" collapse. The top trace shows the base acceleration - the duration of the earthquake of about 0.17 s occupies about 5 mm on the time axis near the beginning of the trace. The pore pressure responses shown in the next two traces were taken from transducers directly beneath the crest. The first was at an initial depth of 125 mm from the crest and was probably in the sliding mass of soil, but very near to the shear zone. The second pore pressure was measured at a depth of about 155 mm from the crest and could be accurately located relative to the slip plane using post test radiographs (see figure 5.5c.). This second transducer was approximately 20 mm beneath the shear zone in the part of the embankment that did not "statically" slip. The first trace shows a small negative pore pressure generated during the earthquake gradually becoming positive as the collapse occurred. The second transducers shows a very different response - a very small pore pressure generated during the quake and then a gradual build up of excess pore pressure to about 9.0 kPa when the failure occurred.

The horizontal displacement at mid height and the crest settlement traces remain steady until the earthquake, when they undergo several millimetres of movement. After the quake, a steady creep is apparent on both traces until the collapse occurs after about 3.5 s.

The cause effect relationships for this failure cannot be understood until further study can be given to pore pressure data in the time after this and other earthquakes. However, it seems likely that this delayed failure was a result of strain softening during the earthquake deformation and/or pore water pressures generated during the earthquake.

7. CONCLUDING REMARKS

The five models tested gave consistent, repeatable results. Furthermore, models of different scale that represent the same prototype agree with each other, adding support to the centrifuge scaling laws. The Newmark Sliding Block Calculation using a rigid plastic soil strength on a distinct slip surface consistently under predicts measured displacements. Shear zones in clay embankments during earthquakes do not tend to form distinct rupture planes. In these models shear zones of 10-30 mm thickness were observed. Hence from small cyclic displacements of less than 1 mm per cycle we would obtain less than 3% to 10% strains. These small strains are not large enough to mobilise the full undrained shear strength, but can result in permanent deformation. Permanent displacements due to stresses below the shear strength must be accounted for in order to improve predictions. Other factors which should be accounted for are the magnification of base accelerations due to resonance of the embankment, and strain softening during the course of the earthquake.

The collapse of model CV 3.5 s after the earthquake resulted in deformations an order of magnitude larger than any measured during the earthquake. This delayed "static" collapse caused by strain softening and/or pore pressure generation during the earthquake may be the most important consideration when designing dams to resist earthquakes. If the delayed failure is due to pore pressure dissipation or redistribution, the 3.5 s scales to about two hours in prototype time.

REFERENCES

Kutter, B. L. (1979) "Behaviour of Embankments under dynamic loading", M. Phil. thesis, Cambridge University.

Kutter, B. L., forthcoming Ph D thesis, Cambridge University

Morgenstern, N. R. and Price, V. E. (1965) "The analysis of the stability of general slip surfaces", Geotechnique, London, England, Vol. 15, pp 79-93.

Morris, D. V. (1979) "The centrifugal modelling of dynamic behaviour", Ph D thesis, Cambridge University

Newmark, N. M. (1965) "Effects of earthquakes on dams and embankments", Geotechnique, London, England, Vol. 15, No. 2, pp 141-156

Sarma, S. K. (1975) "Seismic stability of earth dams and embankments", Geotechnique, London, England, Vol. 25, No. 4, pp 743-761

Sketchley, C. J. (1973) "The behaviour of kaolin in plane strain", Ph D thesis, Cambridge University.

Table I Characteristics of the Models and Corresponding Prototypes

Model	Test No.	Centrifuge Acceleration (g)	Model Height (mm)	Prototype Height (m)	Model Frequency (Hz)	Prototype Frequency (Hz)	"Static" Factor of Safety	Yield Acceleration Coefficient
A	I to III	80	86	6.9	121.9	1.52	1.53	0.20
A	V	100	86	8.6	136.3	1.36	1.22	0.09
A	Static failure	122	86	10.5	-	-	1.0	0.0
B	I to V	80	86	6.9	121.9	1.52	1.53	0.20
C	I to IV	35.6	193	6.9	54.2	1.52	1.53	0.20
C	V	44.5	193	8.6	60.6	1.36	1.22	0.09
D	I to III	35.6	193	6.9	54.2	1.52	1.53	0.20
E	I to V	35.6	202	7.2	81.3	2.28	1.46	-

TABLE II Summary of Data

Test	Acceleration (g)	(Earthquake Accn) / (Centrifuge Accn) Base (%)	(Earthquake Accn) / (Centrifuge Accn) Crest (%)	Crest Settlement (mm)	Horizontal Displacements +Z Side** (mm)	Horizontal Displacements -Z side ** (mm)
AI	80	3.8	7	0.003	0.003	0.002
AII	80	13.5	23.4	0.218	0.209	0.166
AIII	80	24.5	33.5	2.025	2.030	1.58
AIV	100	4.2	8.4	0.098	0.055	0.056
BI	80	25.1	31.2	2.681	1.985	2.155
BII	80	2.1	3.3	0.001	0.004	0.003
BIII	80	7.9	14.0	0.009	0.004	0.009
BIV	80	20.6	31.2	1.215	0.835	1.123
BV	80	23.3	34.0	1.633	1.240	1.531
CI	35.6	2.5	3.3	0.012	-	0.012
CII	35.6	9.5	12.7	0.023	-	0.00
CIII	35.6	14.1	18.6	0.188	-	0.187
CIV	35.6	17.9	24.3	1.224	-	1.22
CV	44.5	17.7	24.0	9.0	-	7.6
DI	35.6	21.8	28.0	3.254	3.221	2.205
DII	35.6	3.3	7.0	0.009	0.0003	0.004
DIII	35.6	21.7	32.1	3.027	4.71	2.42
EI	35.6	19	24	0.1	0.059	0.055
EII	35.6	21	27	0.45	0.363	0.257
EIII	35.6	23	34	0.69	0.593	0.347
EIV	35.6	23	34	0.66	0.601	0.343
EV	35.6	23	34	0.61	0.554	0.312

** +Z side and -Z side refer to faces of the model. The +Z side is the face nearest the leading edge of the centrifuge.

TABLE III

Summary of Sliding Block Predicted Displacements and a Comparison with Measured Horizontal Displacements at mid-height of the models.

TEST	Measured Displacements (mm)		Predicted Displacements (mobilised strength = C_u)			Predicted Displacements (mobilised strength = 0.9 C_u)		
	+Z	-Z	k_y*	+Z Displacement	-Z Displacement	k_y*	+Z Displacement	-Z Displacement
BI	1.985	2.155	0.2	0.162	0.256	0.15	0.623	0.837
CIII	-	0.187	0.2	0.001	0.000	0.15	0.048	0.085
CV	-	7.6	0.09	6.54	5.49	0.03	23.5	18.1
DI	3.221	2.205	0.2	0.066	0.208	0.15	0.622	1.493

*k_y = Yield Acceleration/Centrifuge Acceleration

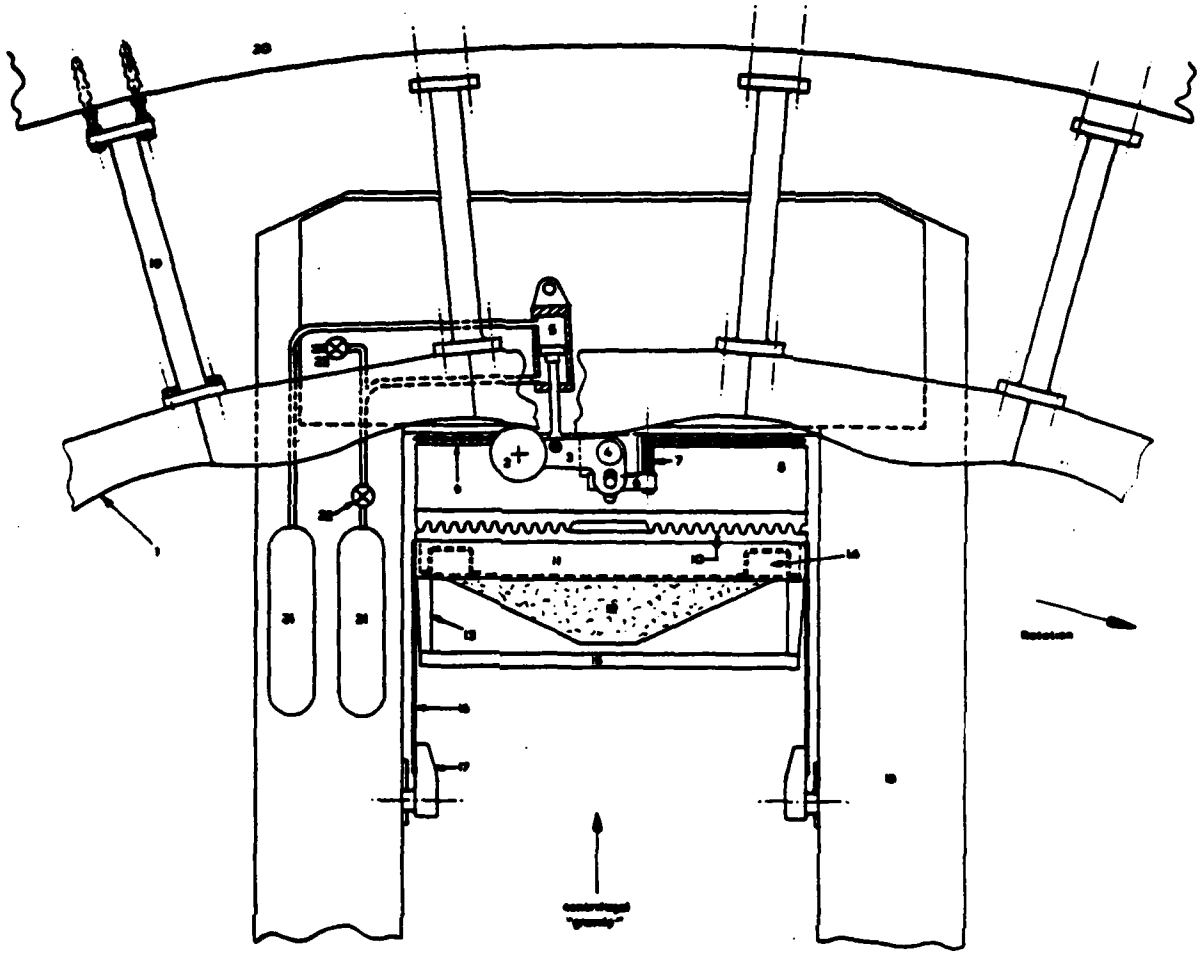

Fig. 3.1a Schematic view of Bumpy Road Apparatus looking downward into centrifuge pit. The specimen container is shown in its swung up and seated position.

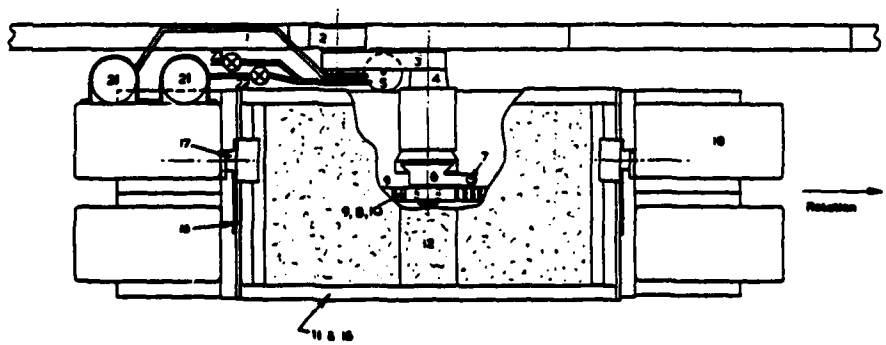

Fig. 3.1b Schematic view of Bumpy Road Apparatus looking radially outward from centrifuge axis. There is a cutaway view through the swinging specimen container.

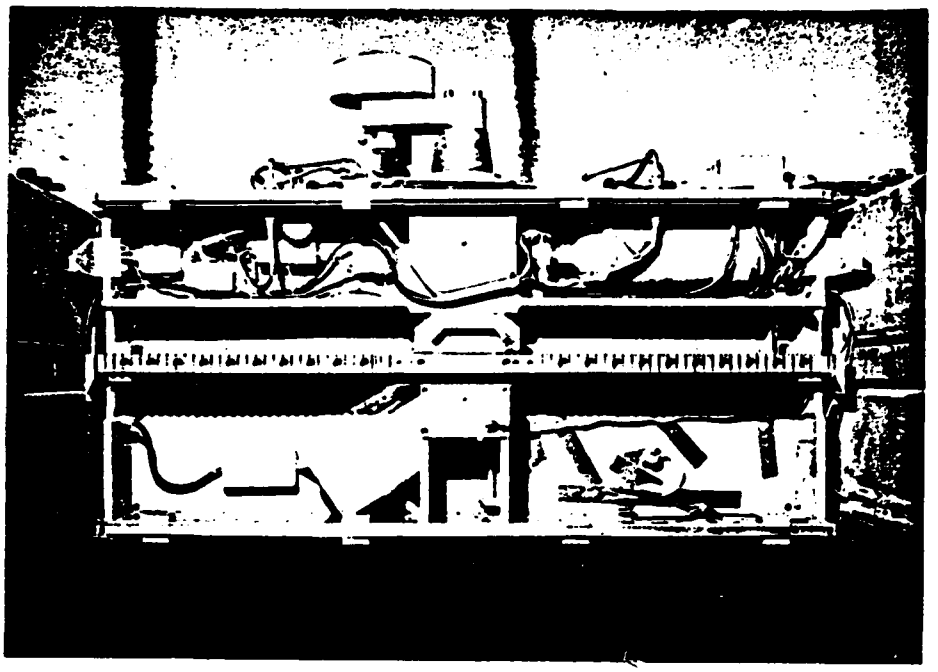

Fig. 3.2a Photograph of Bumpy Road Actuator looking outward from centrifuge axis. The swinging specimen container is not shown.

Fig. 3.2b A tangential view over the top of the centrifuge arm. The steel track is held on the wall by brackets that are enclosed in streamlining. The nylon wheel is being held clear of the track by the pneumatic jack.

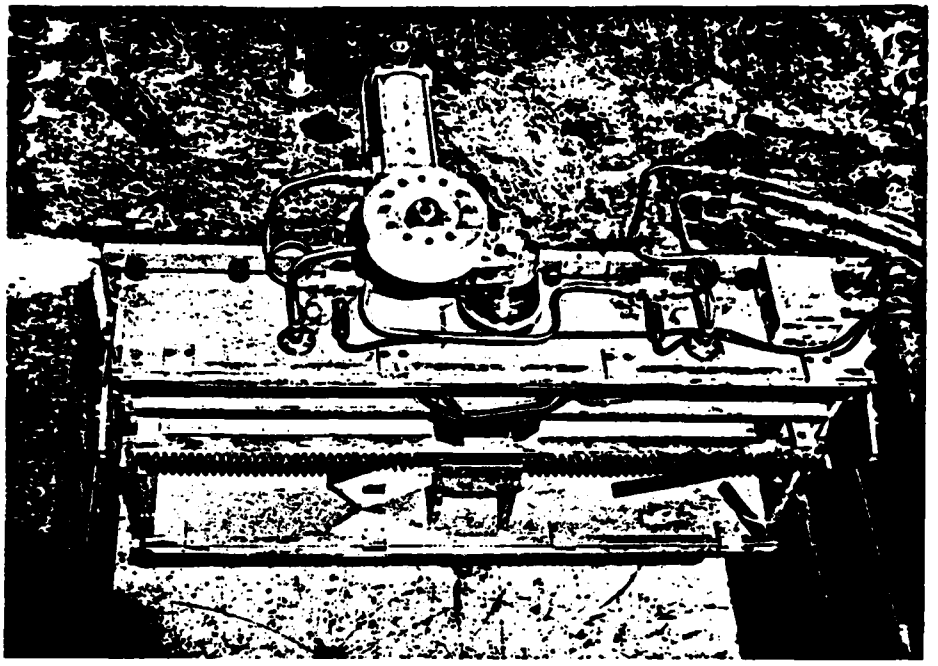

Fig. 3.2c View of Actuator looking downward into centrifuge pit

Fig. 3.2d A view of the swinging specimen container. The container pivots about the bearings attached to the flexible straps. The package would swing up to the left. Vibrations are imposed to the container in and out of the picture.

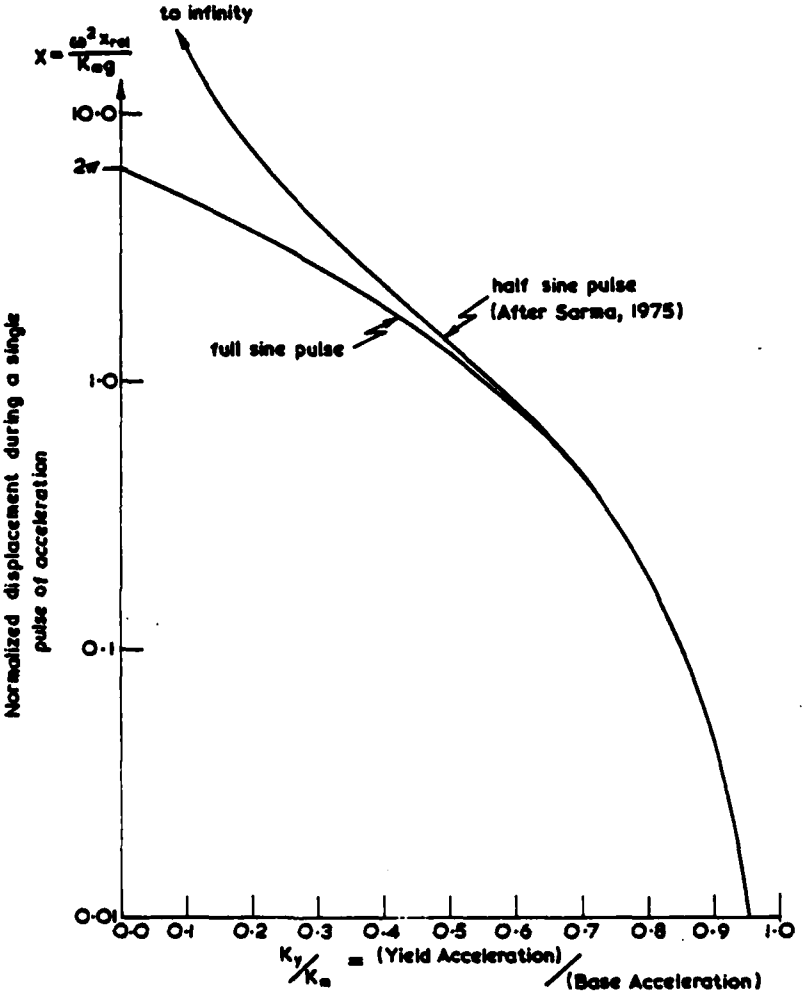

Fig. 4.1 Relationship between normalised displacement and the ratio of yield and base accelerations. (From Kutter, 1979).

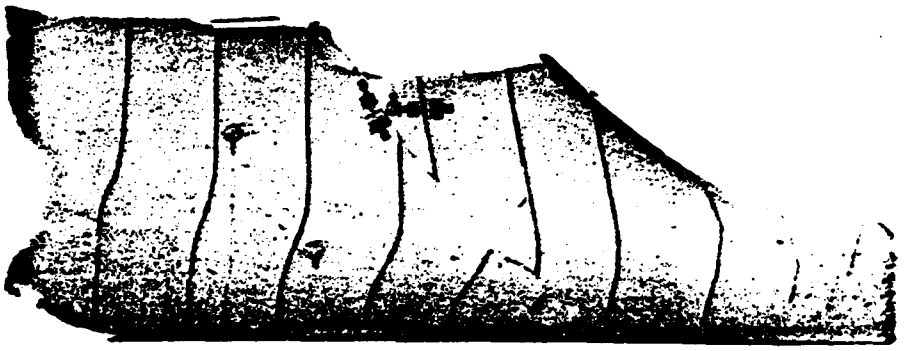

Fig. 4.2 Radiograph of Model BK-5 (From Kutter, 1979)

Fig. 4.3a

ASSUMED CONDITIONS FOR SENSITIVITY ANALYSIS

* SLIDING BLOCK ANALYSIS
* 2:1, COHESIVE SLOPE
* YIELD ACCELERATION, $K_y g = 0.1g$
* 1 Hz SINE PULSE
* HORIZONTAL BASE VIBRATION

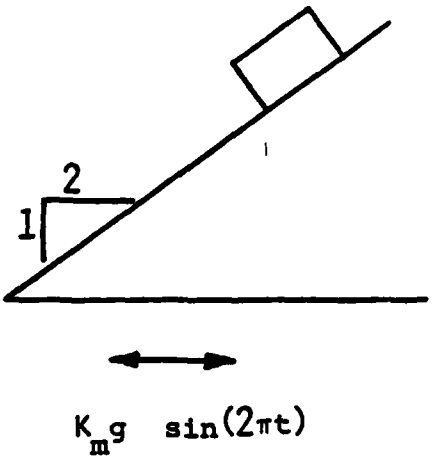

Fig. 4.3b.

PREDICTED AND ACTUAL DISPLACEMENTS IF PREDICTIONS ARE BASED ON A 5% OVERESTIMATION OF SOIL STRENGTH

CASE	K_m	K_y/K_m	PREDICTED DISPLACEMENT	ACTUAL DISPLACEMENT	PERCENTAGE ERROR
I	0.11	0.9	1.0 mm	17 mm	1600.%
II	0.5	0.2	400 mm	460 mm	13 %

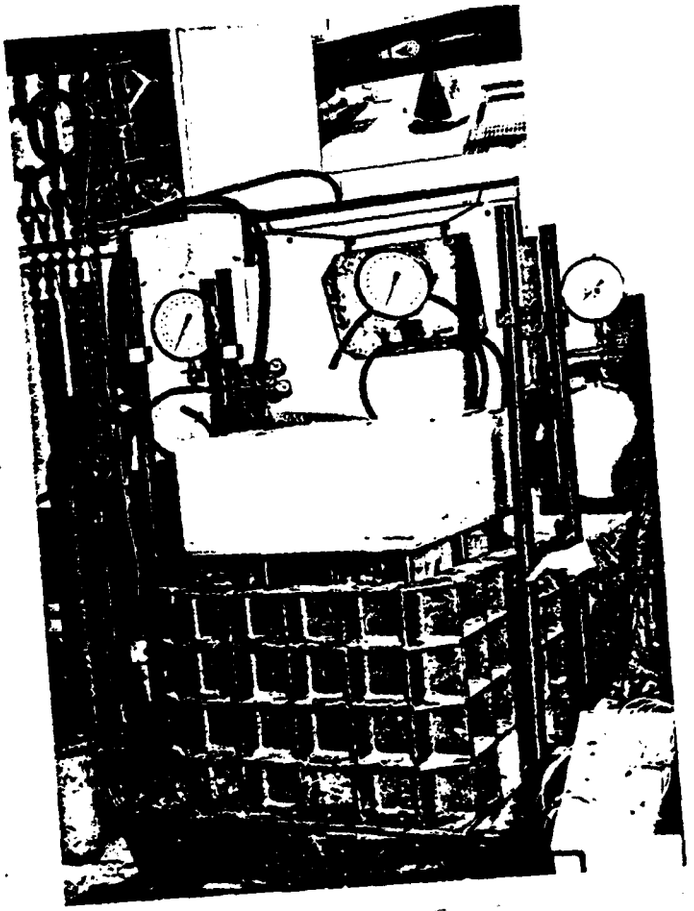

Fig. 5.1 A rectangular block of kaolin is extruded before trimming. The block has been consolidated to a pressure of 124 kPa.

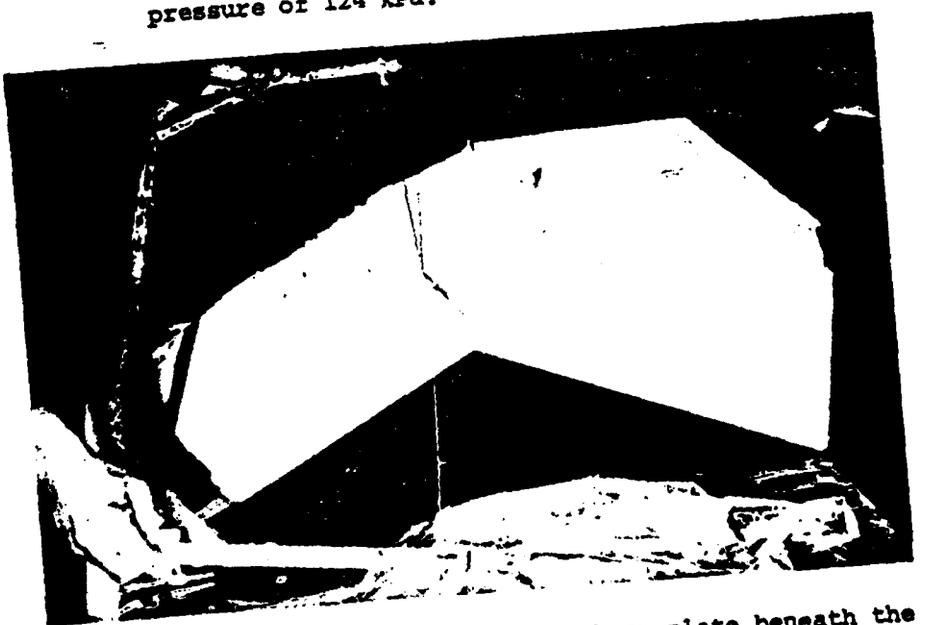

Fig. 5.2. A template is bolted to the base plate beneath the clay and the profile is trimmed using cutting wire.

Fig. 5.3

MODEL B
Dimensions and Instrumentation

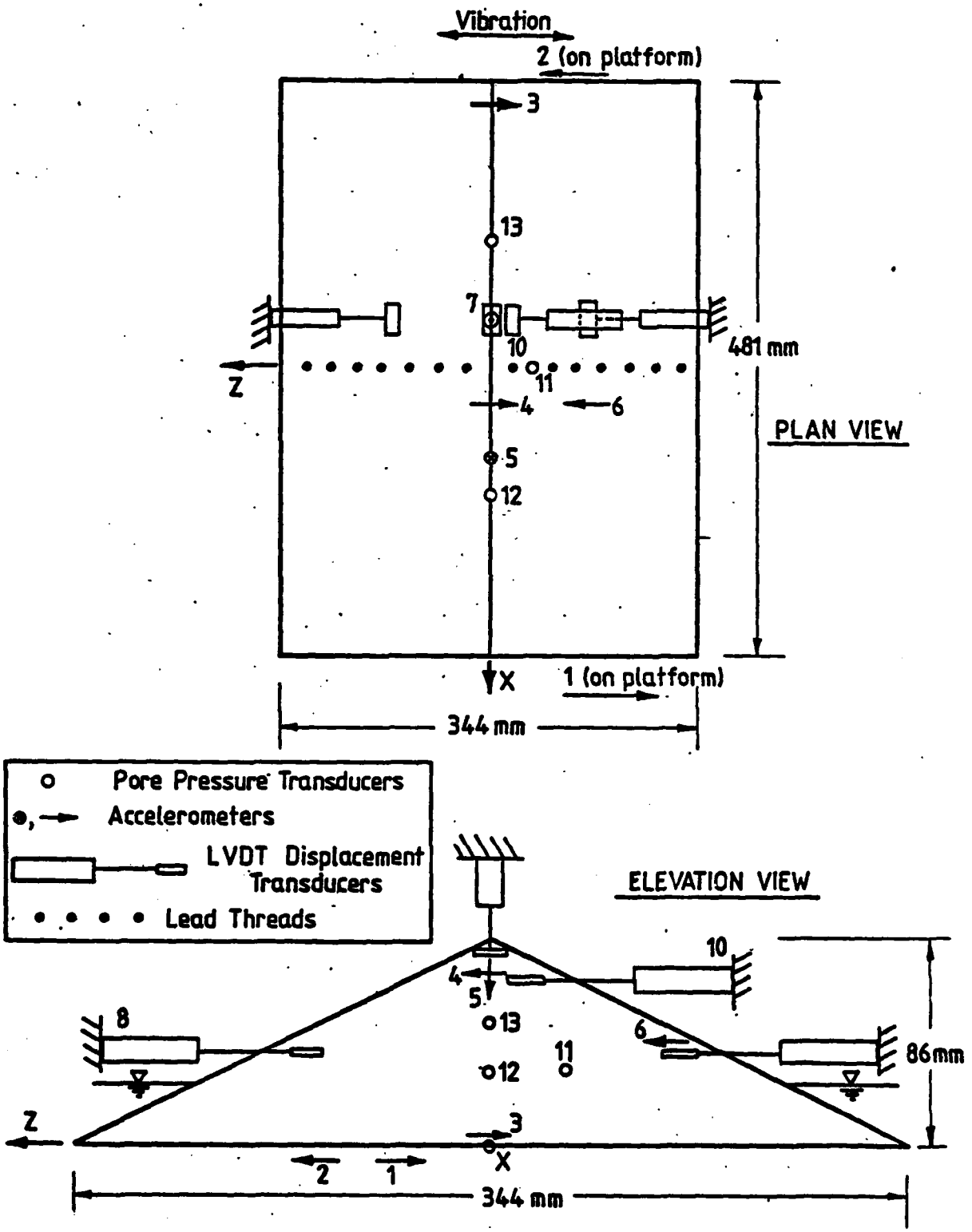

Fig. 5.4

MODEL D
Dimensions and Instrumentation

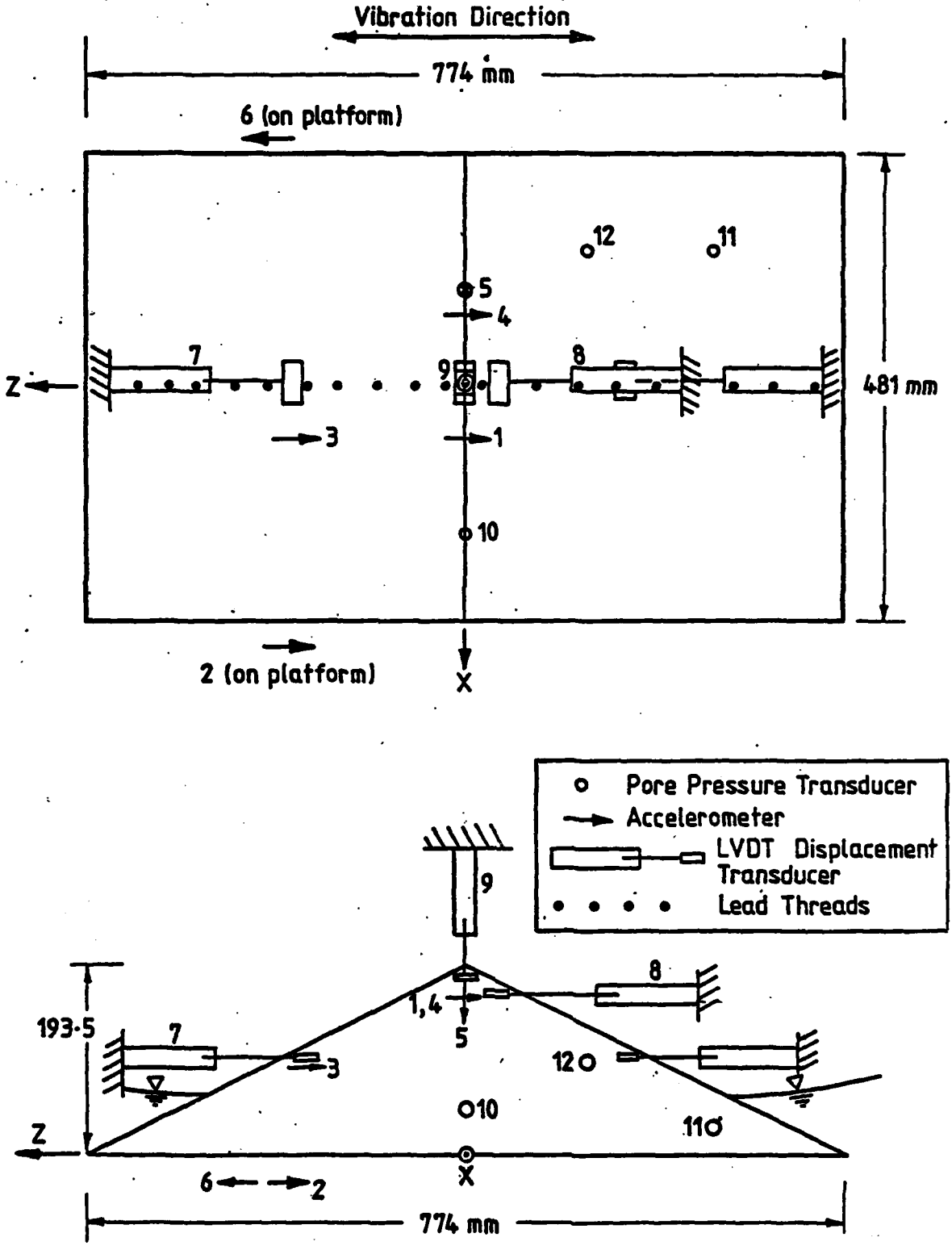

Fig. 5.5a Radiograph of Model A afrer testing. The curvature of the threads in the left half of the photograph occurred primarily during vibration. The slip on the right side occurred at 122g.

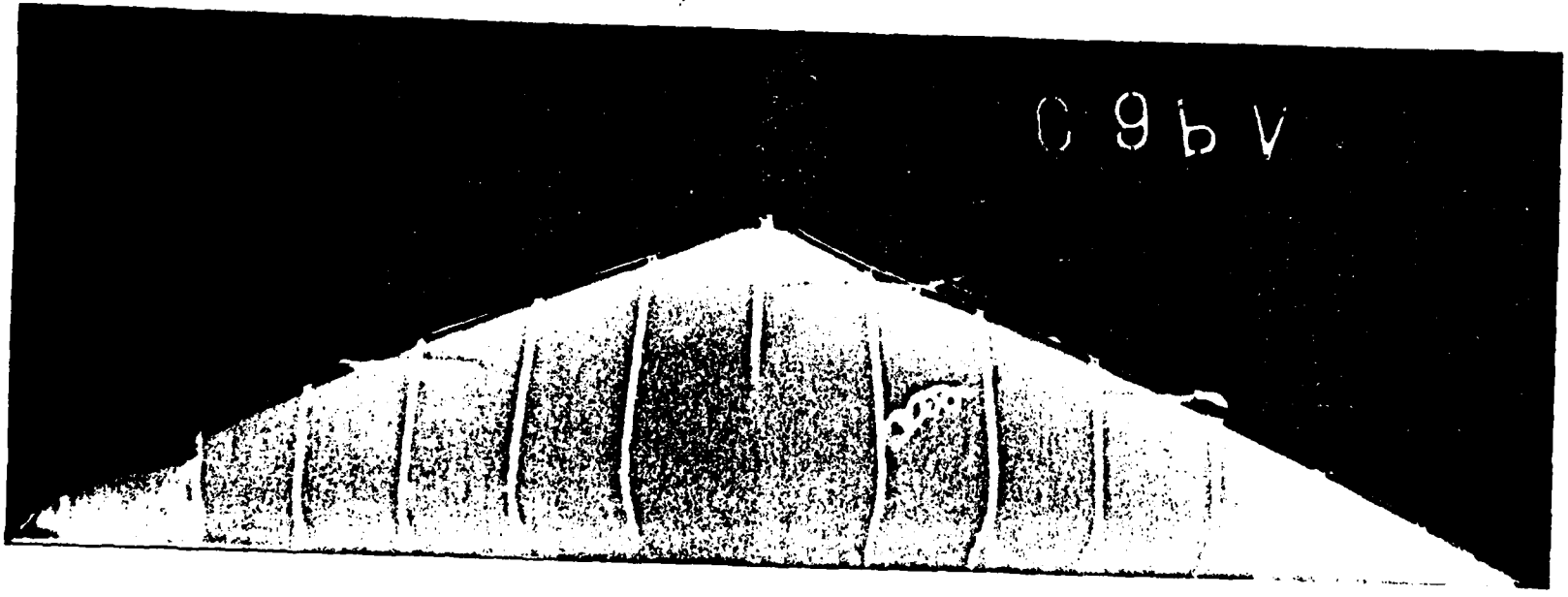

Fig. 5.5b. Radiograph of Model B after testing. Severe earthquake induced distortion is visible on both sides of the embankment. A small toe failure is apparent on the left toe. The LVDT anchors for measuring horizontal displacements are apparent and a pore pressure transducer is visible in the interior of the specimen.

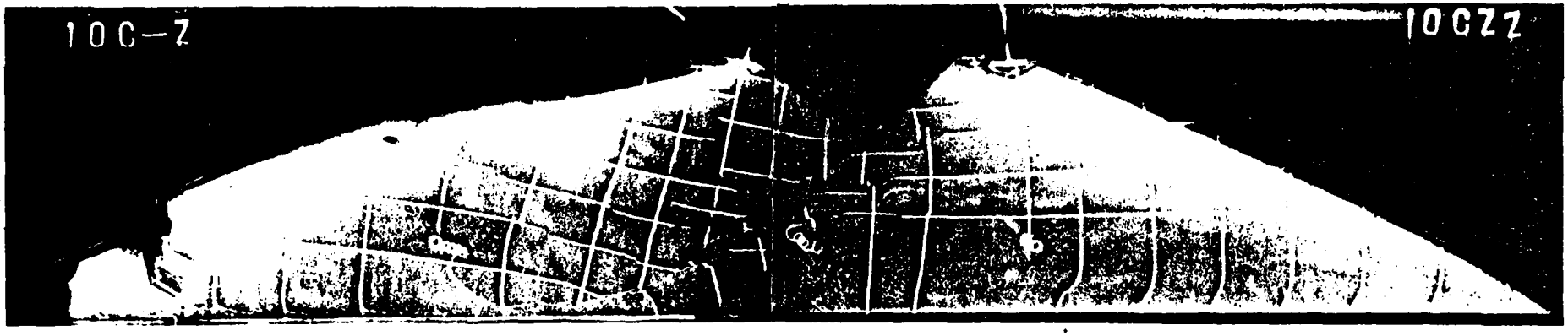

Fig. 5.5c Radiograph of Model C. Earthquake induced distortion is apparent on the right side of this specimen. The catastrophic collapse toward the left occurred 3.5 s after earthquake CV.

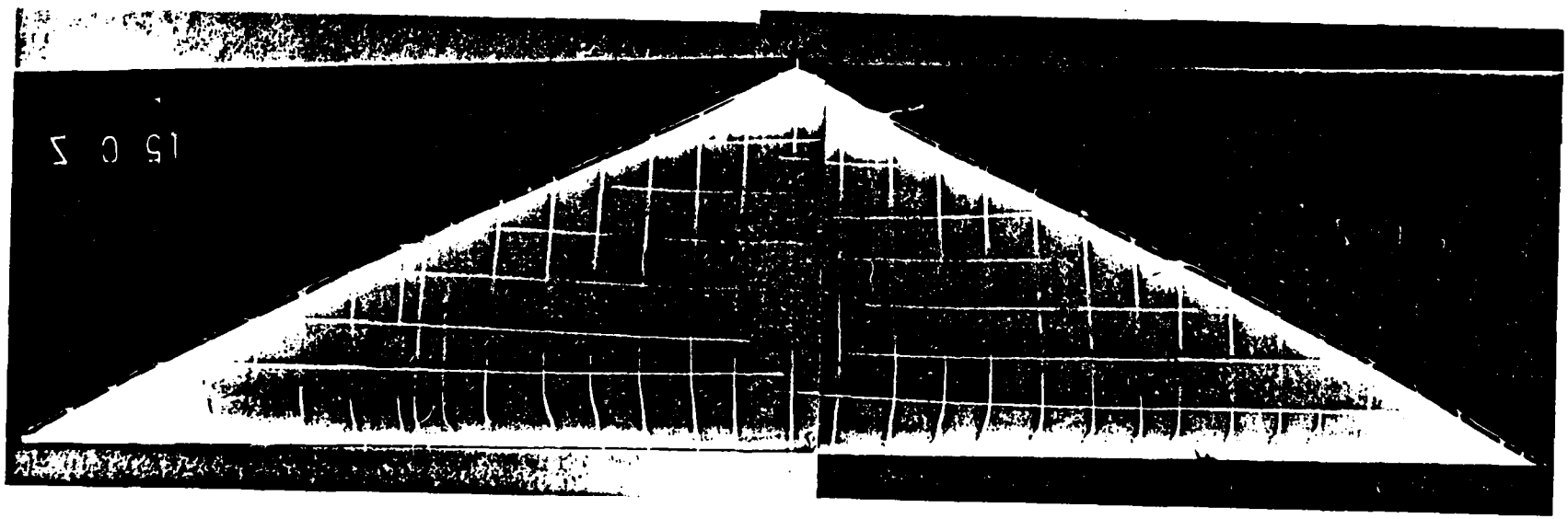

Fig. 5.5d Model D Earthquake induced distortion apparent near the base of the specimen.

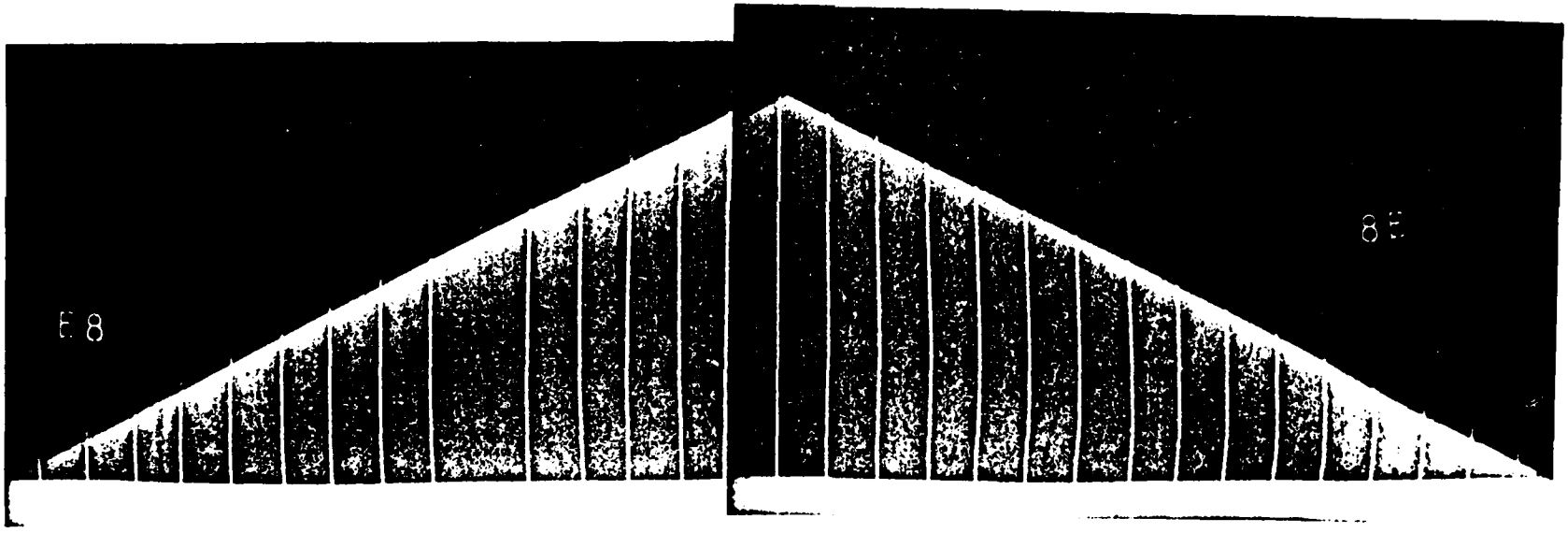

Fig. 5.5e Radiograph of Model E. Very slight internal deformation is detectable by observing the consistent curvature of the lead threads.

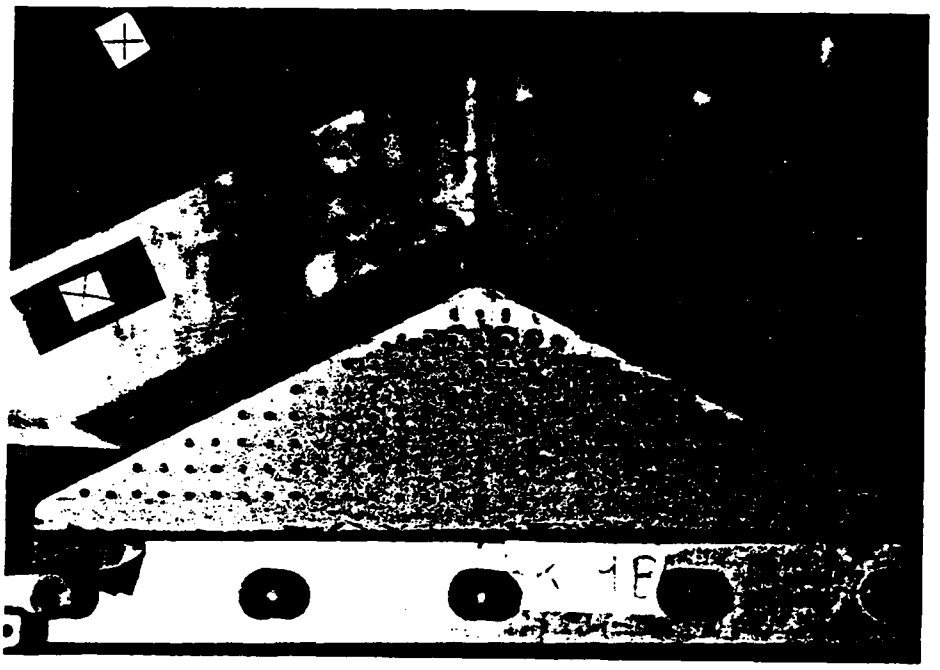

Fig. 5.6a Model B photographed in flight before earthquakes (80g)

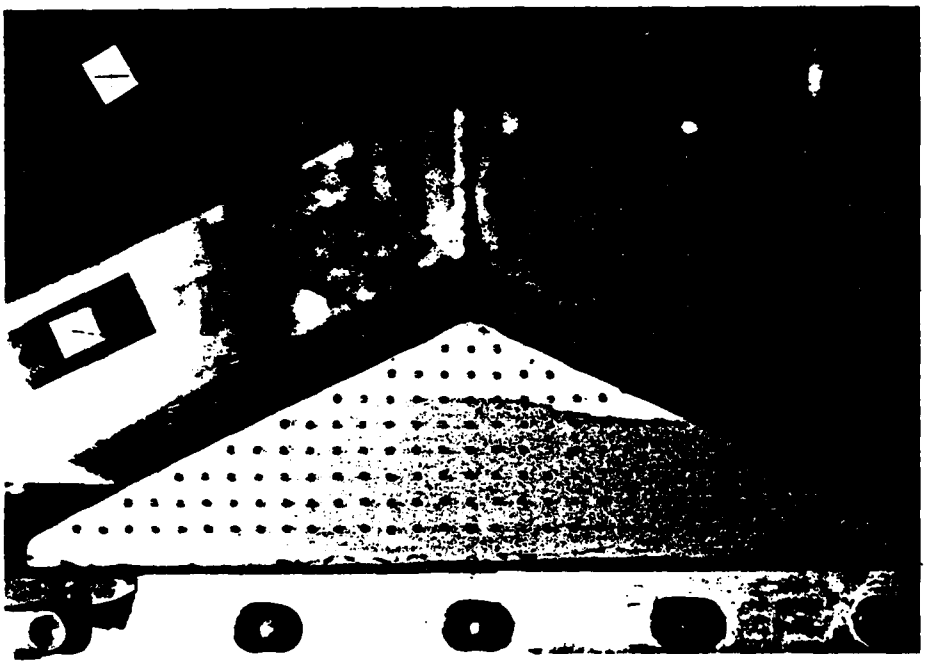

Fig 5.6b Model B photographed in flight after all earthquakes (80g). Holding a straight edge against the surface markers will reveal distortion of the embankment. More accurate measurements on the film measuring machine would enable determination of volumetric and shear strains of this section.

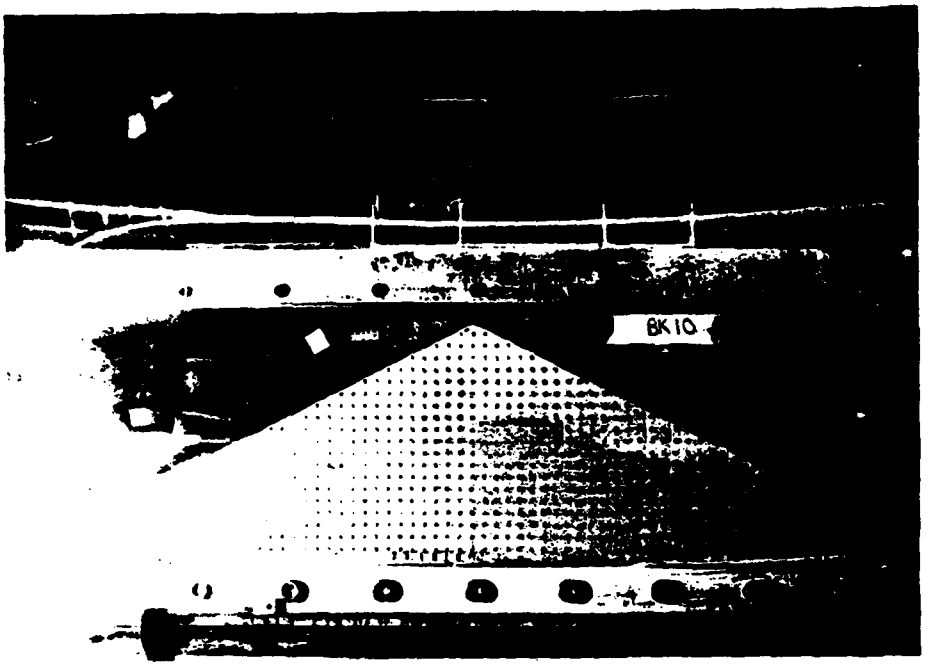

Fig. 5.7a Model C photographed in flight at 35.6g, before any earthquake.

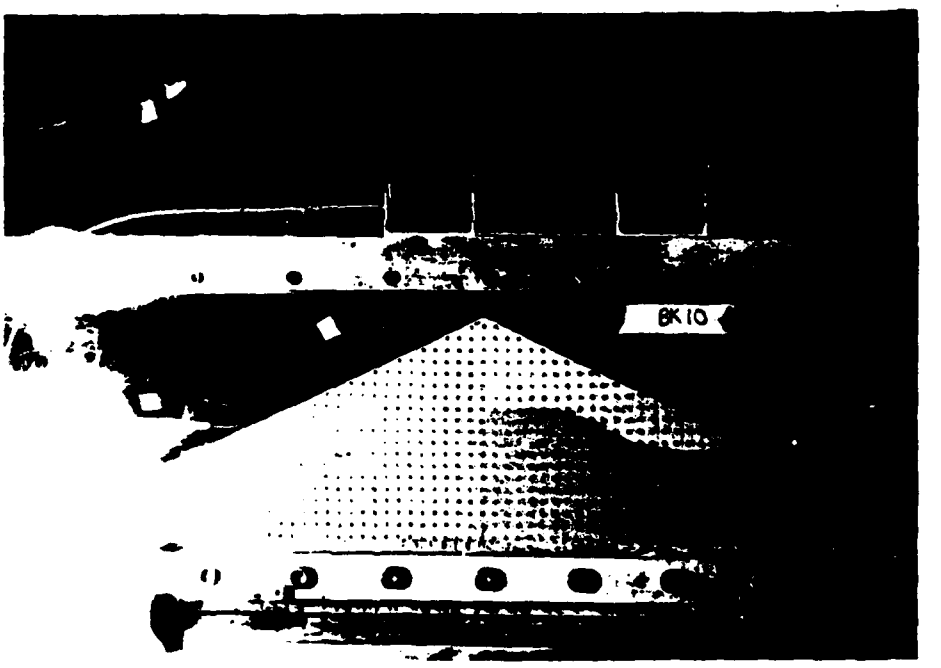

Fig. 5.7b Model C photographed in flight at 44.5g after earthquake CIV, just before earthquake CV.

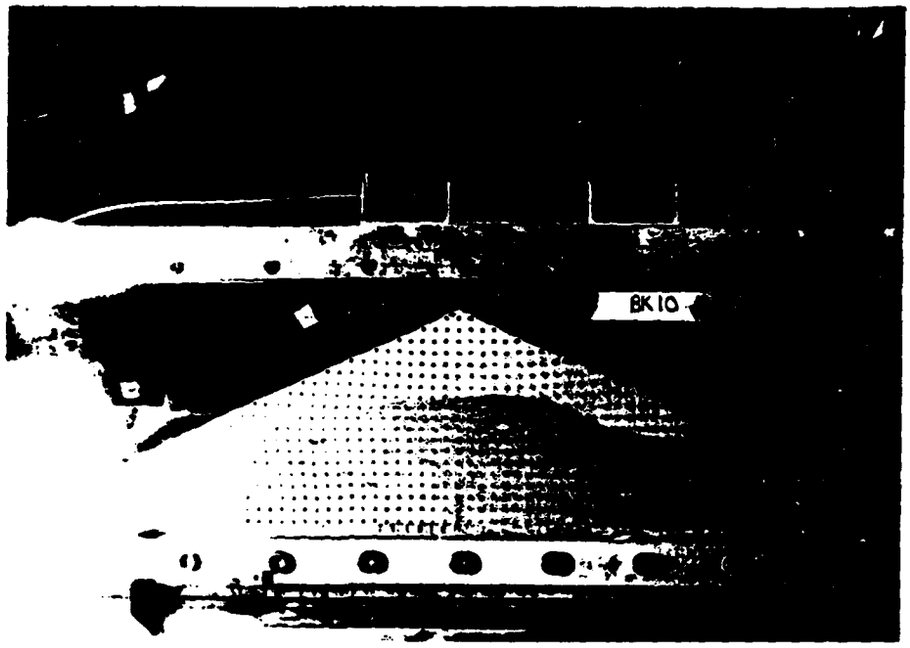

Fig. 5.7c Model C photographed in flight at 44.5g after 5 pulses of earthquake CV.

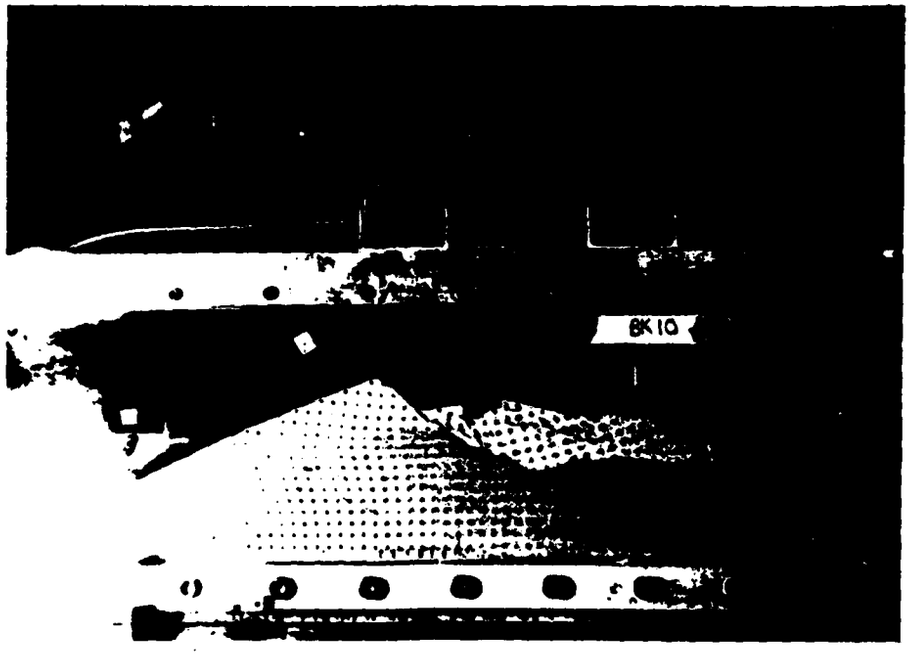

Fig. 5.7d Model C photographed in flight at 44.5g, several seconds after earthquake CV.

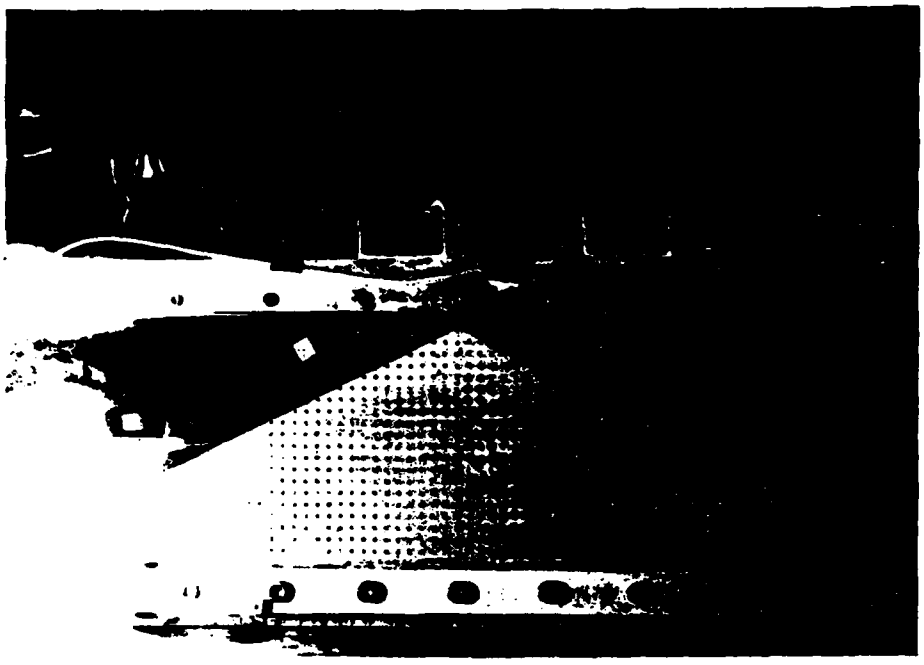

Fig. 5.8a Model D photographed in flight at 35.6g, before any earthquakes.

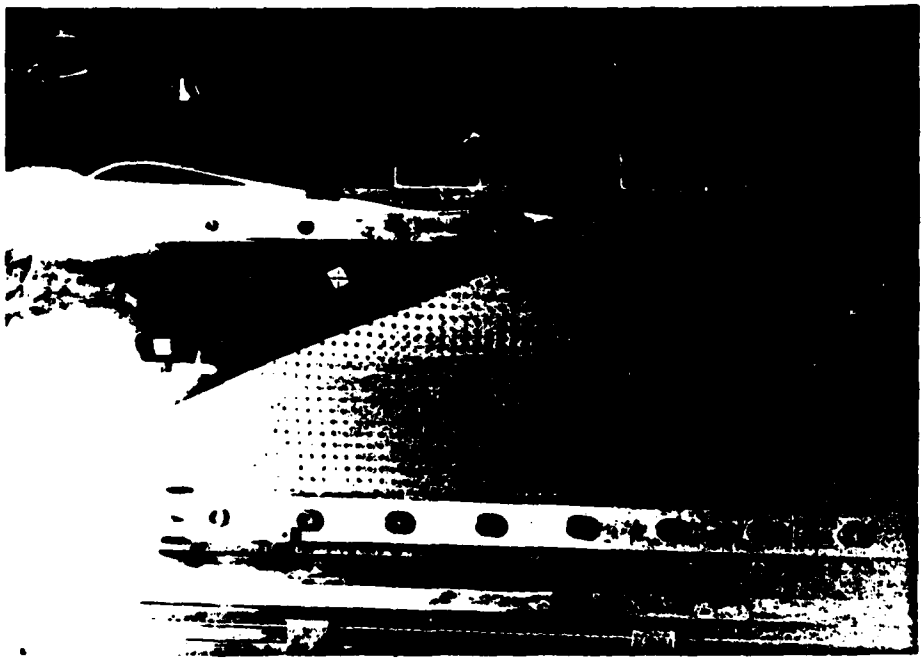

Fig. 5.8b Model D photographed in flight at 35.6g, after all 3 earthquakes.

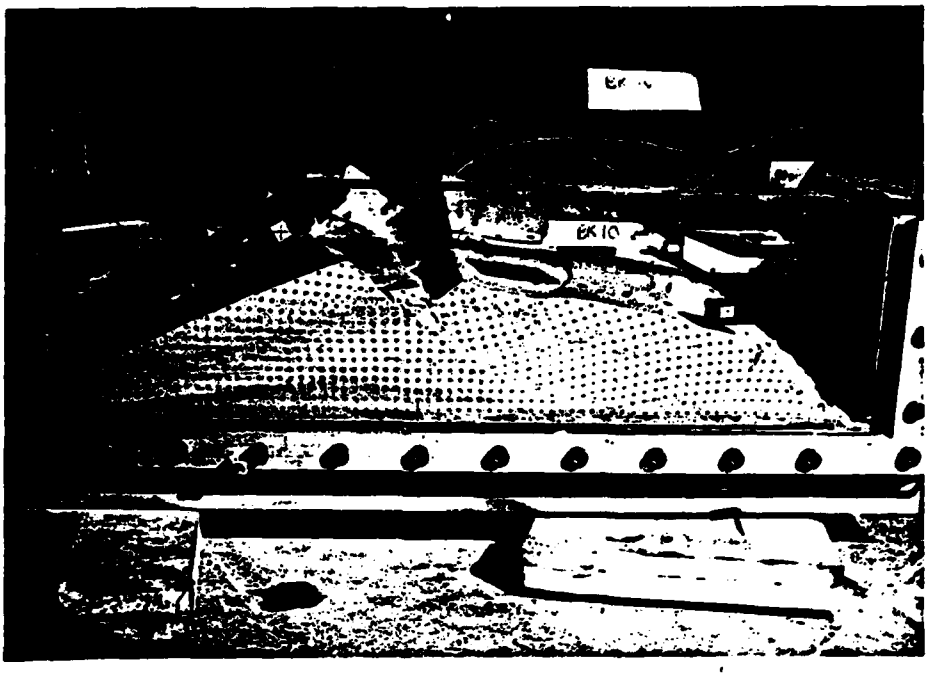

Fig. 5.9a Model C after removing from centrifuge

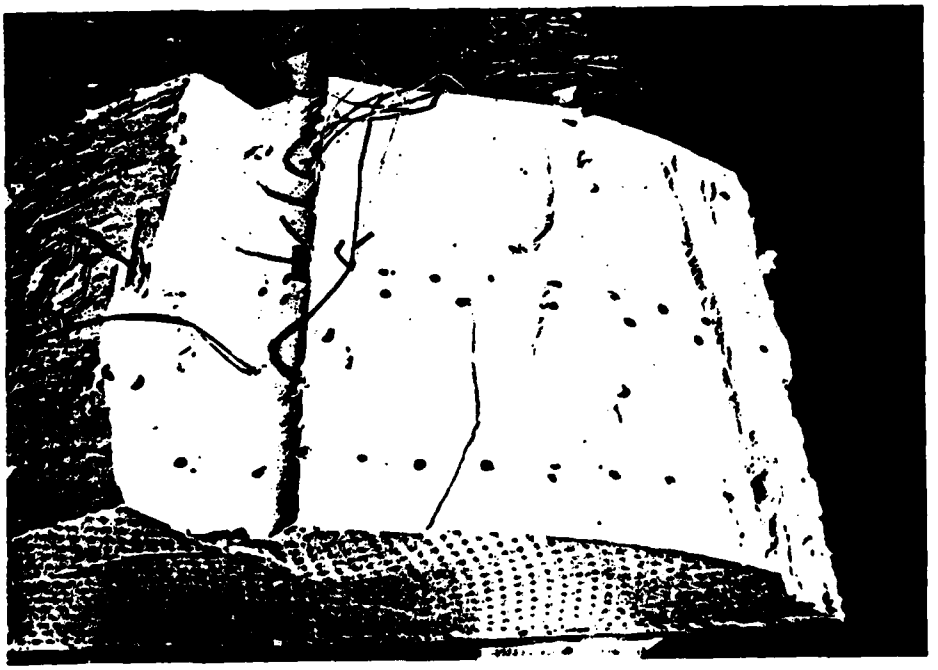

Fig. 5.9b Model C after removing from swinging container

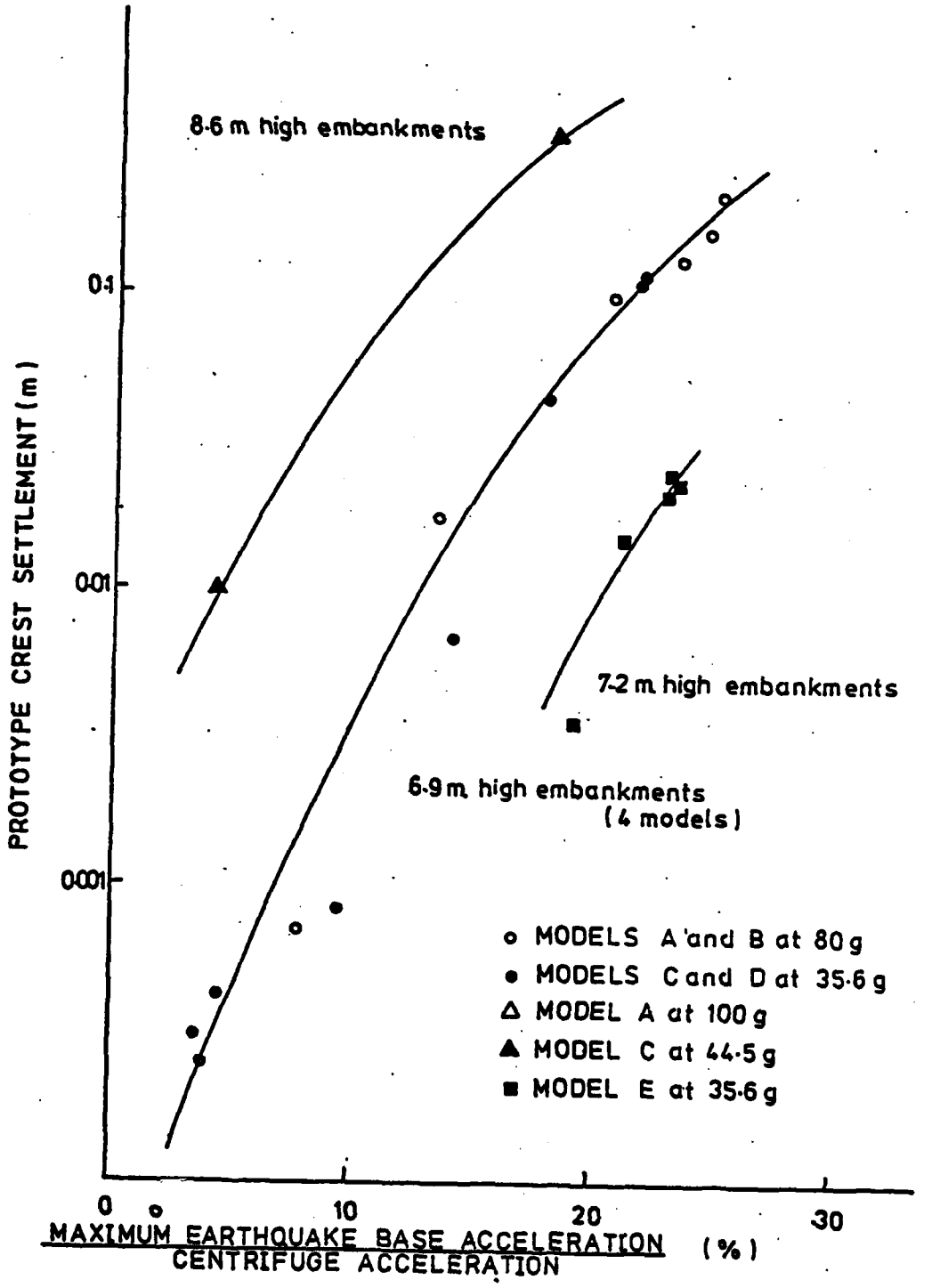

Fig. 6.1 Experimental relation between prototype crest settlement and the maximum earthquake acceleration coefficient

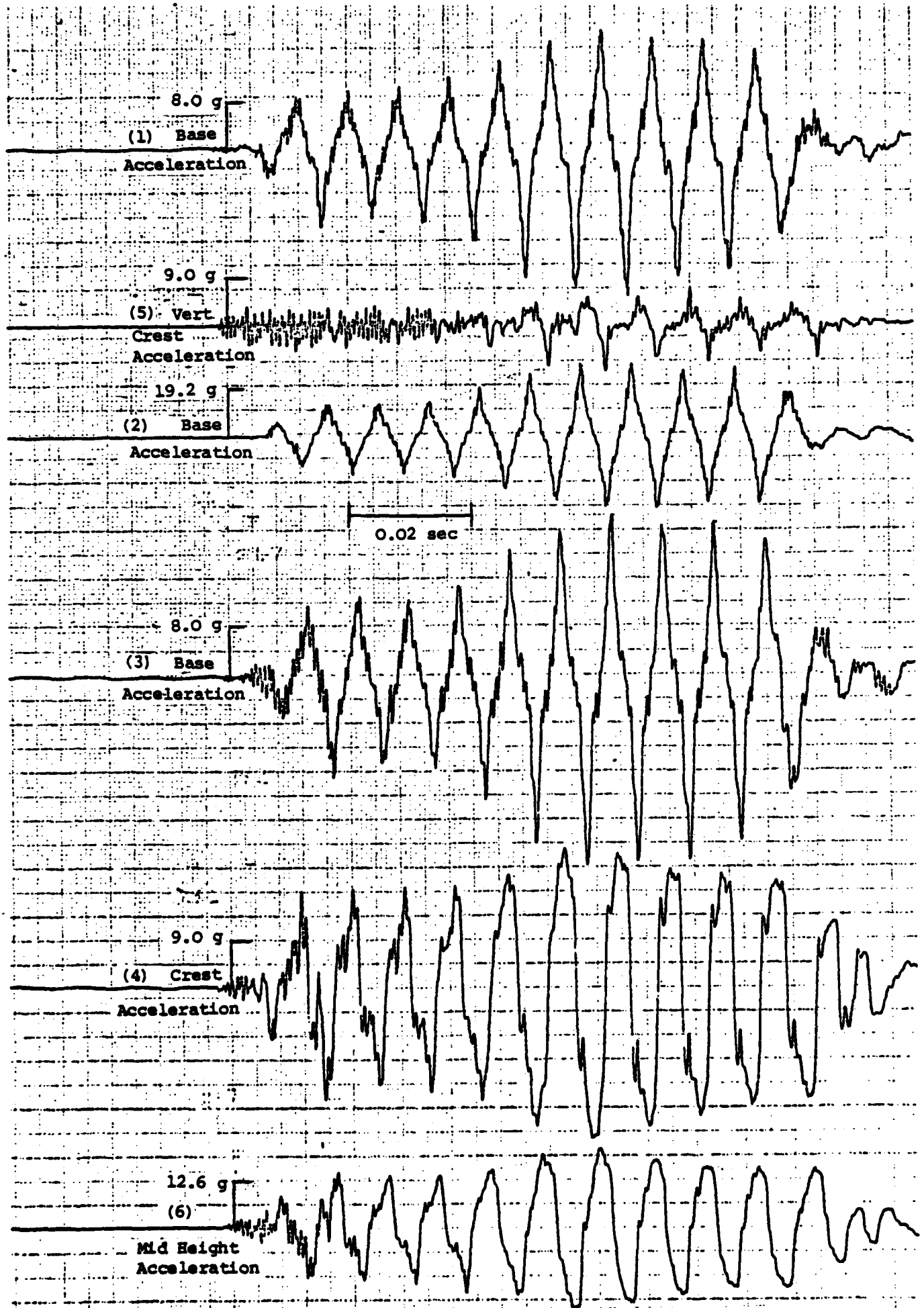

Figure 6.2a Some Data from test BI.

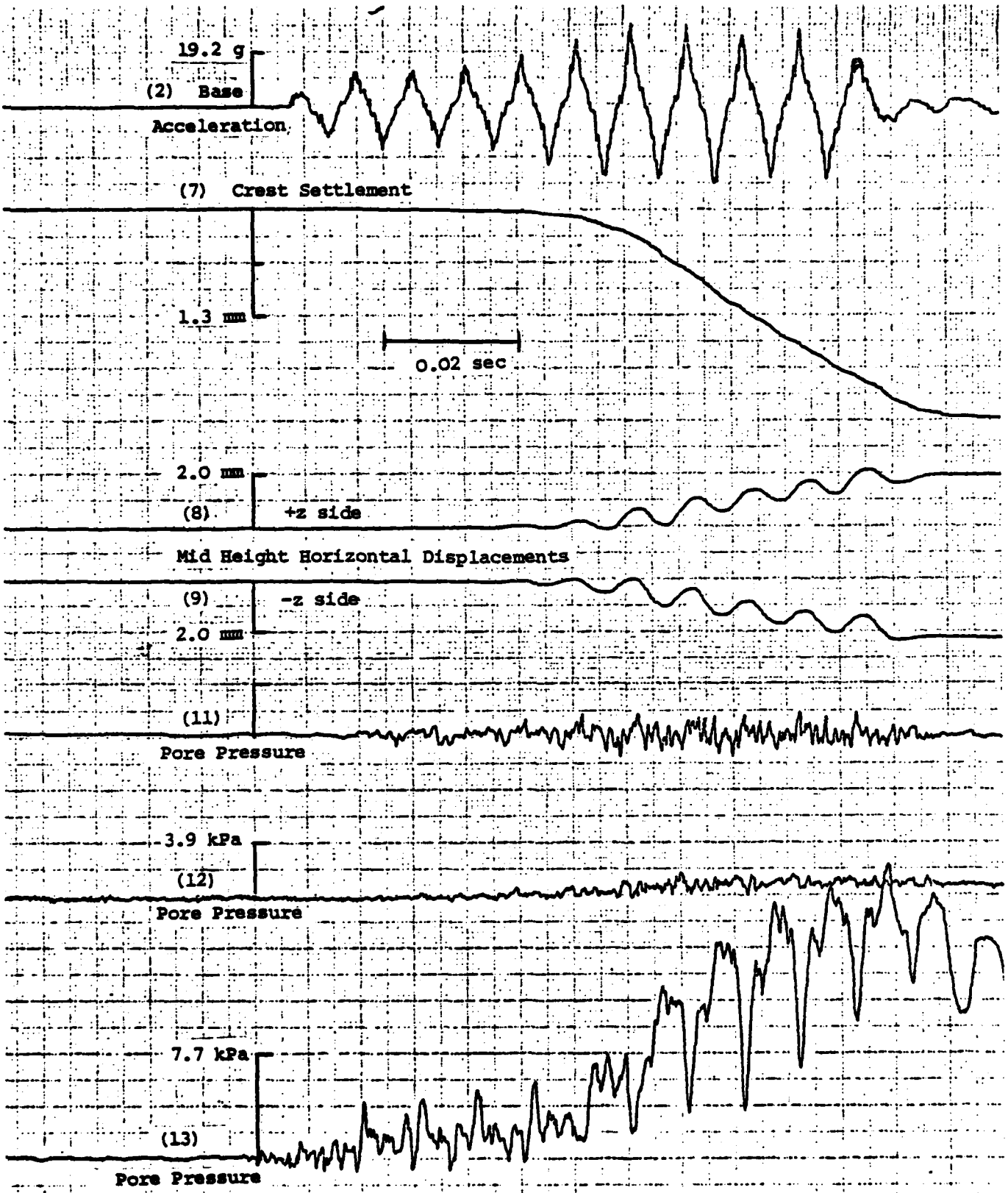

Figure 6.2b Some Data from test BI.

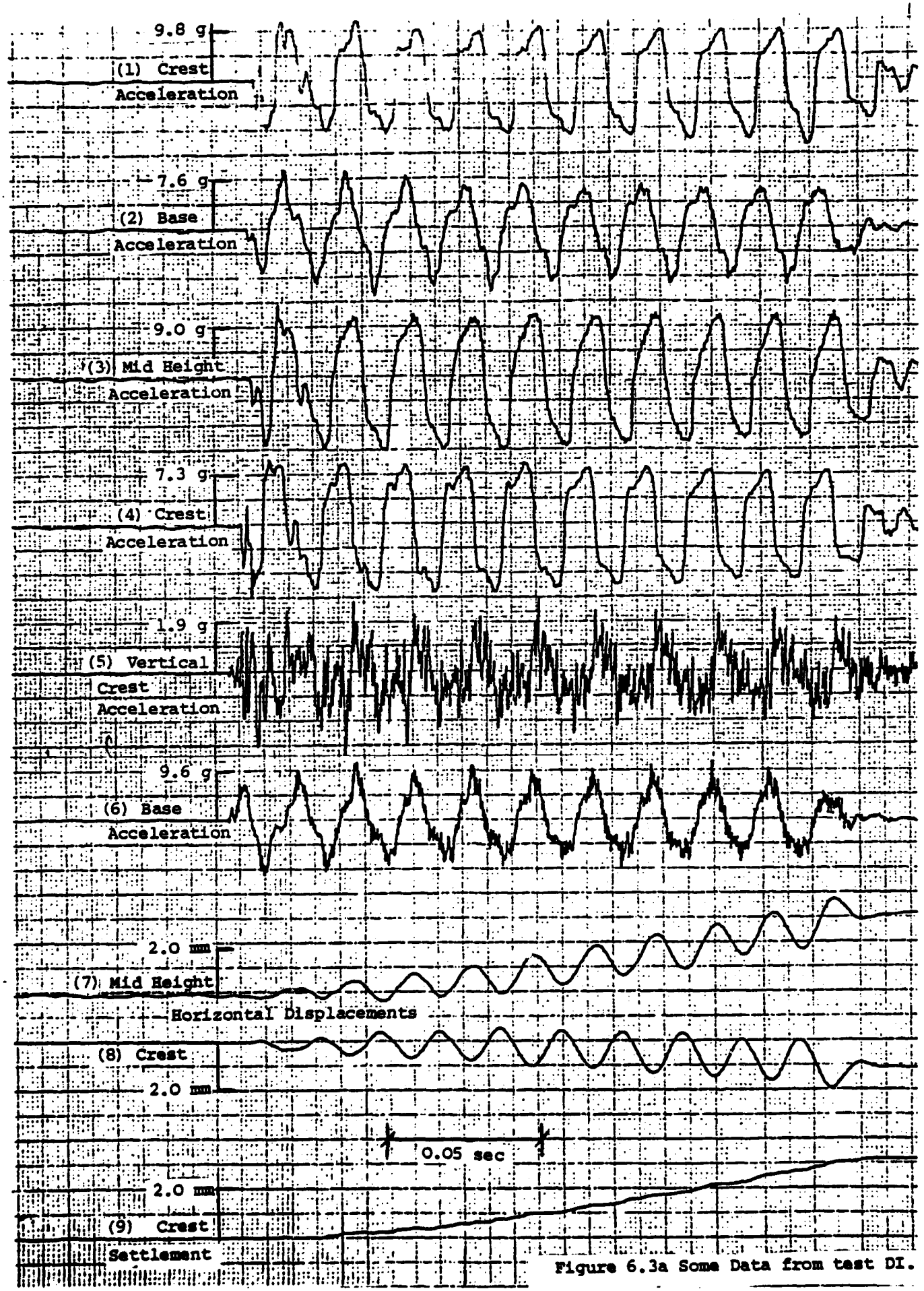

Figure 6.3a Some Data from test DI.

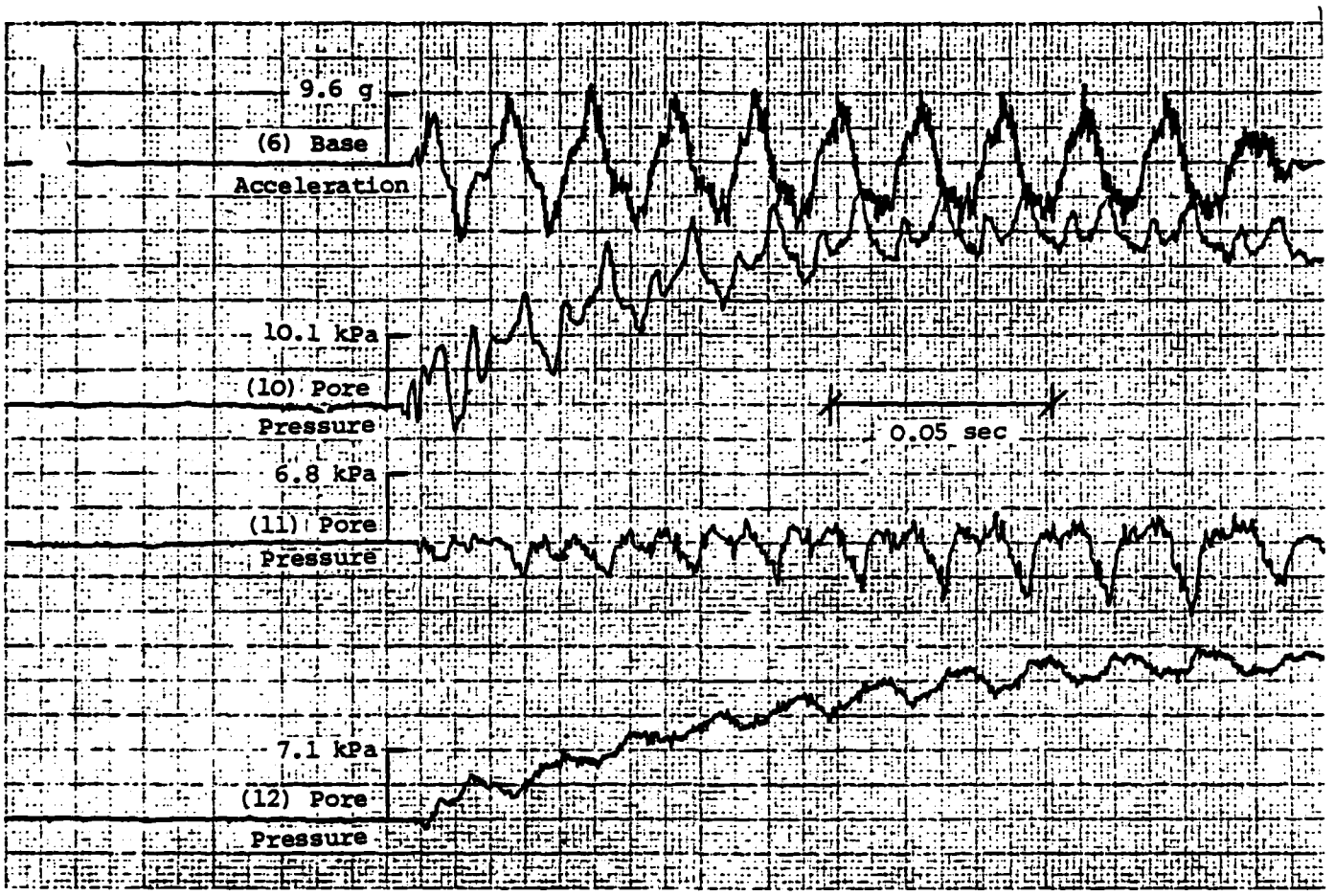

Figure 6.3b Some Data from test DI.

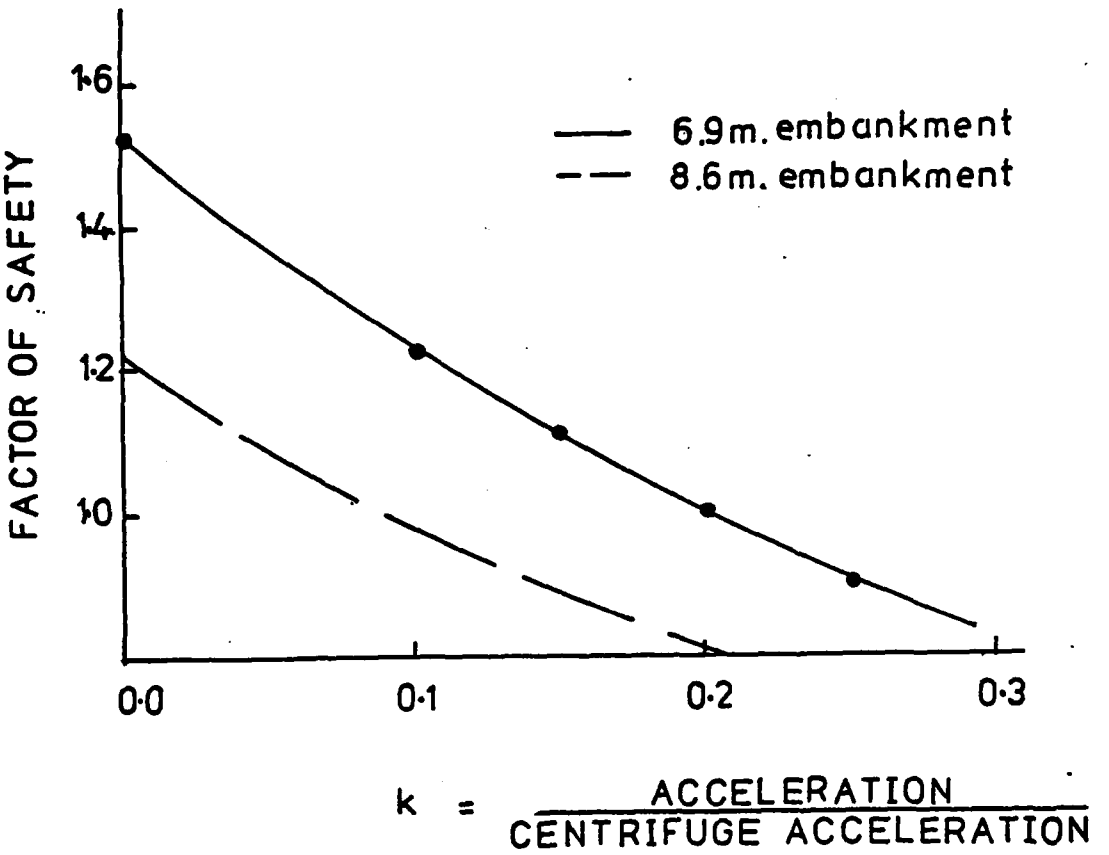

Fig. 6.4 Results of method of slices slip circle analysis on 6.9 m high prototypes and extrapolated curve for 8.6 m high prototypes.

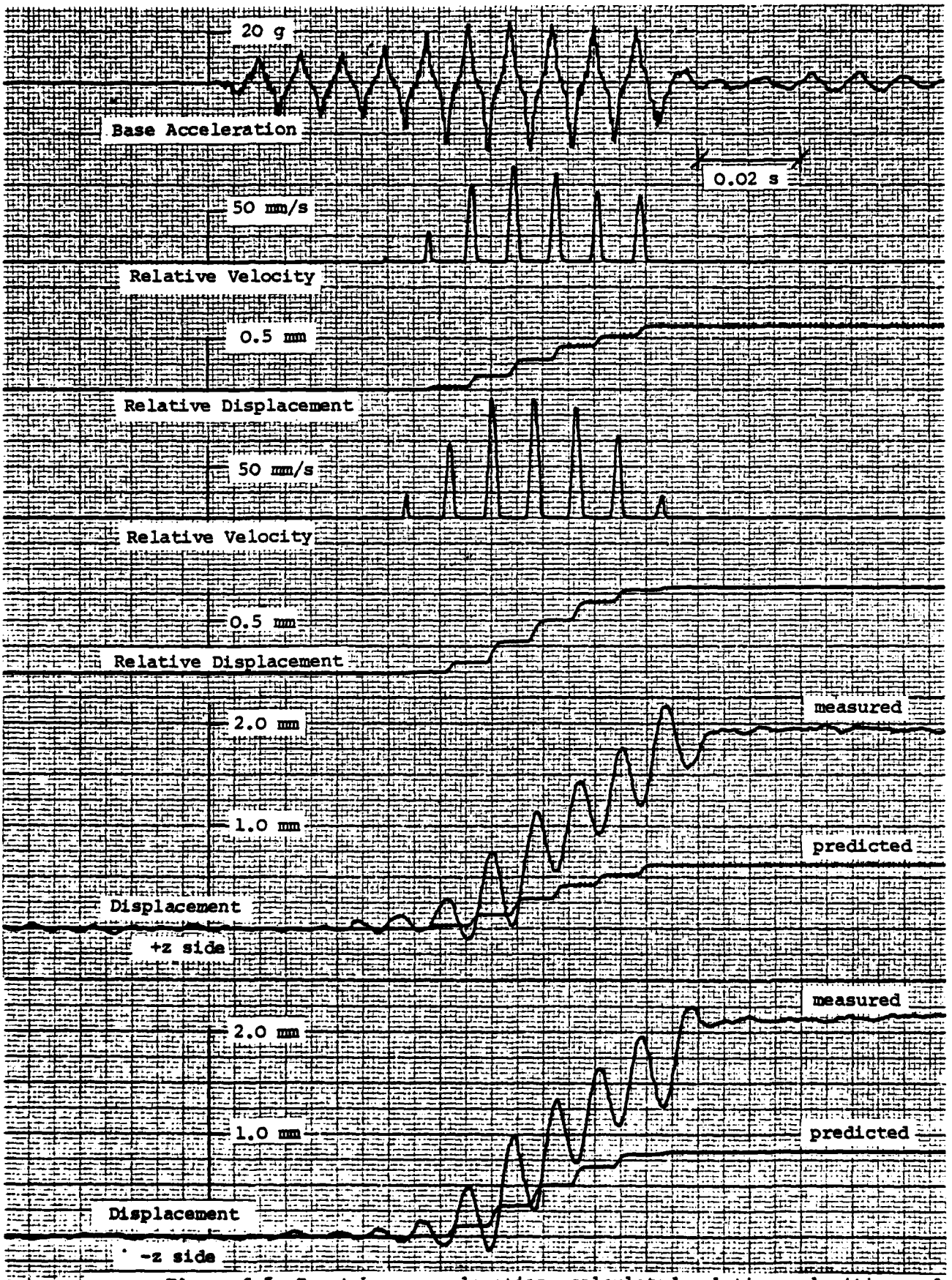

Figure 6.5 Input base acceleration, calculated relative velocities and relative displacements and comparison with measured displacements for test BI. For calculations the strength was assumed to be 0.9 C_u and the corresponding yield acceleration is 0.15(80 *g*)=12 *g*.

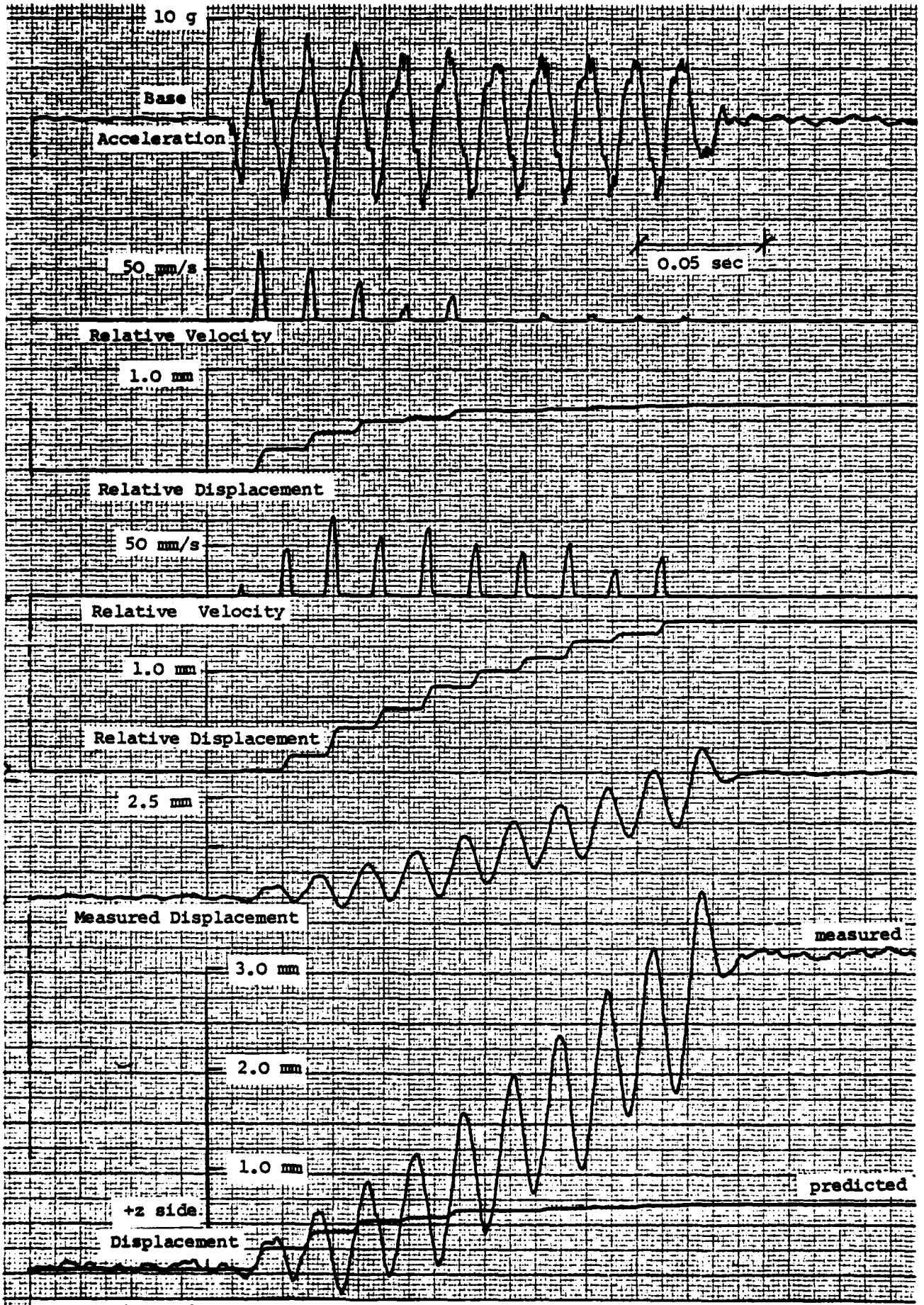

Figure 6.6 Input base acceleration, calculated relative velocities and relative displacements and comparison with measured displacements for test DI. For calculations the strength was assumed to be 0.9 C_u and the corresponding yield acceleration is 0.15(35.6 g)=5.33 g.

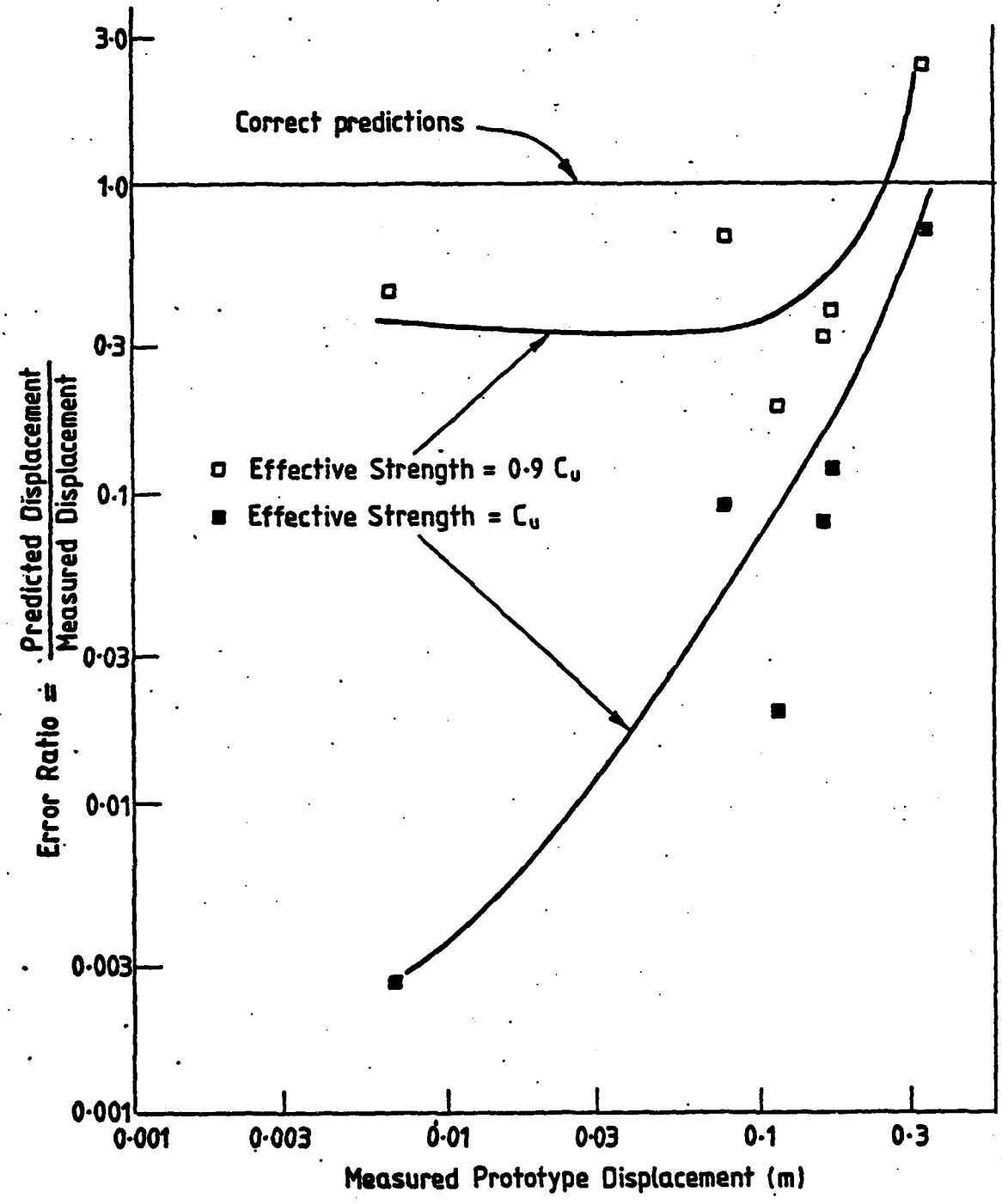

Fig. 6.7. Relation between the error ratio for displacement predictions and total prototype displacement for some of the tests.

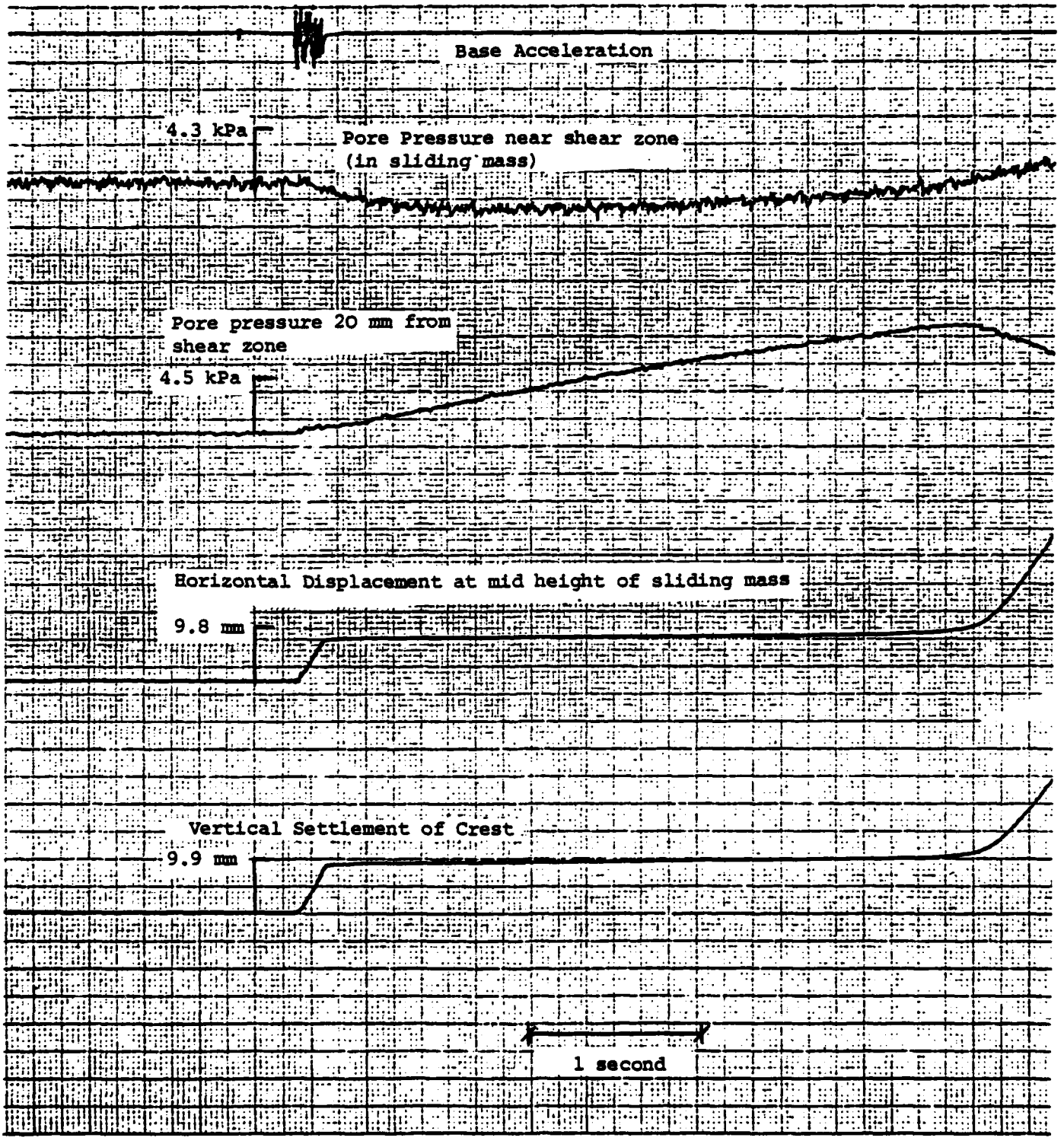

Figure 6.8 Some transducer readings during and after test CV